



Originally published as:

Schurr, B., Asch, G., Rosenau, M., Wang, R., Oncken, O., Barrientos, S., Salazar, P., Vilotte, J. P. The 2007 M7.7 Tocopilla northern Chile earthquake sequence: Implications for along-strike and downdip rupture segmentation and megathrust frictional behavior. - *Journal of Geophysical Research*, 117, B5

DOI: [10.1029/2011JB009030](https://doi.org/10.1029/2011JB009030)

The 2007 M7.7 Tocopilla northern Chile earthquake sequence: Implications for along-strike and downdip rupture segmentation and megathrust frictional behavior

B. Schurr,¹ G. Asch,¹ M. Rosenau,¹ R. Wang,¹ O. Oncken,¹ S. Barrientos,² P. Salazar,³ and J.-P. Vilotte⁴

Received 14 November 2011; revised 27 March 2012; accepted 28 March 2012; published 16 May 2012.

[1] In 2007 a M7.7 earthquake occurred near the town of Tocopilla within the northern Chile seismic gap. Main shock slip, derived from coseismic surface deformation, was confined to the depth range between 30 and 55 km. We relocated ~ 1100 events during six months before and one week after the main shock. Aftershock seismicity is first congruent to the main shock slip and then it spreads offshore west and northwest of Mejillones Peninsula (MP). Waveform modeling for 38 aftershocks reveals source mechanisms that are in the majority similar to the main shock. However, a few events appear to occur in the upper plate, some with extensional mechanisms. Juxtaposing the Tocopilla aftershocks with those following the neighboring 1995 Antofagasta earthquake produces a striking symmetry across an EW axis in the center of MP. Events seem to skirt around MP, probably due to a shallower Moho there. We suggest that the seismogenic coupling zone in northern Chile changes its frictional behavior in the downdip direction from unstable to mostly conditionally stable. For both earthquake sequences, aftershocks agglomerate in the conditionally stable region, whereas maximum inter-seismic slip deficit and co-seismic slip occurs in the unstable region. The boundary between the unstable and conditionally stable zones parallels the coastline. We identify a similar segmentation for other earthquakes in Chile and Peru, where the offshore segments break in great $M > 8$ earthquakes, and the onshore segments in smaller $M < 8$ earthquakes. Using critical taper analysis, we demonstrate a causal relationship between varying slip behavior on the interface and forearc wedge anatomy that can be attributed to spatial variations in the rate-dependency of friction.

Citation: Schurr, B., G. Asch, M. Rosenau, R. Wang, O. Oncken, S. Barrientos, P. Salazar, and J.-P. Vilotte (2012), The 2007 M7.7 Tocopilla northern Chile earthquake sequence: Implications for along-strike and downdip rupture segmentation and megathrust frictional behavior, *J. Geophys. Res.*, *117*, B05305, doi:10.1029/2011JB009030.

1. Introduction

[2] There are some concepts of subduction thrust fault segmentation, both along strike and in the dip direction that are regularly invoked. Along strike it is often assumed that large subduction earthquakes repeatedly break segments separated by barriers. Segments that have not been broken for a longer time relative to the convergence rate

are termed seismic “gaps” [McNally, 1983; Nishenko, 1985]. This concept has been used for first order, long-term subduction earthquake forecast. However, the persistency as well as the nature of barriers (and hence segmentation) is still unclear. In the dip direction, subduction thrust faults are usually divided into an updip aseismic, a central seismogenic and a downdip transitional part according to the frictional properties of the subduction thrust interface [Hyndman *et al.*, 1997]. Some recent large earthquakes, however, have seriously challenged both concepts. The 2010 Maule-Chile earthquake, although somehow filling a “known” seismic gap [Madariaga *et al.*, 2010], left behind by the 1835 earthquake, overlapped with neighboring ruptures to the north (the 1928 and 1985 events) and to the south (the great 1960 earthquake) [Lorito *et al.*, 2011]. The M7.8 2010 Mentawai earthquake slowly ruptured the updip, unbroken part left behind by the 2007 M8.5 Sumatran earthquake [Newman *et al.*, 2011]. This unbroken part of the seismogenic zone had

¹Helmholtz Centre Potsdam, GFZ German Research Centre for Geoscience, Potsdam, Germany.

²Servicio Sismológico, Universidad de Chile, Santiago, Chile.

³Departamento de Ciencias Geológicas, Universidad Católica del Norte, Antofagasta, Chile.

⁴Institut de Physique du Globe de Paris, Paris, France.

Corresponding author: B. Schurr, Helmholtz Centre Potsdam, GFZ German Research Centre for Geoscience, Telegrafenberg, D-14473 Potsdam, Germany. (schurr@gfz-potsdam.de)

Copyright 2012 by the American Geophysical Union.
0148-0227/12/2011JB009030

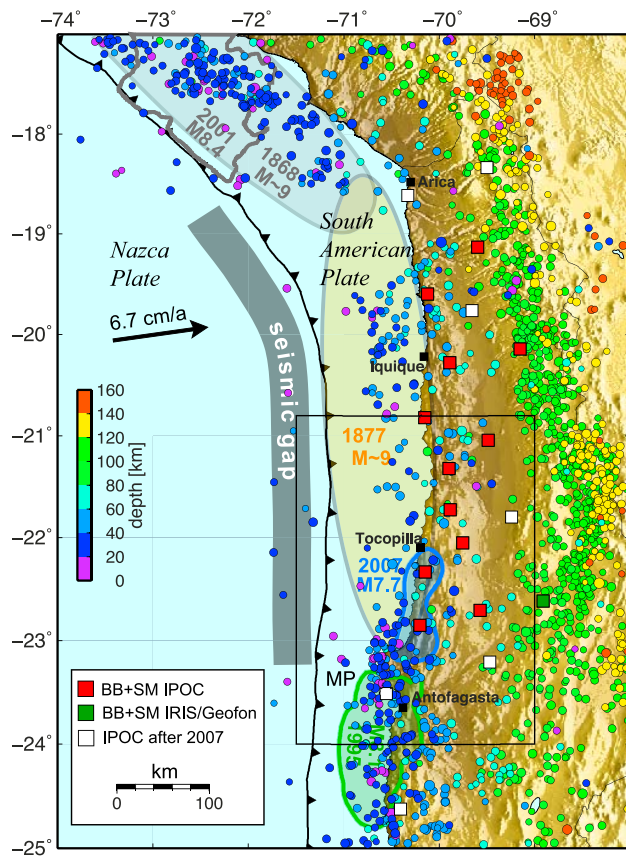


Figure 1. The central South American subduction zone and the IPOC seismic network. Red squares indicate sites of broadband/strong motion seismographs that were operating at the time of the 2007 Tocopilla earthquake, white squares are sites that were built afterwards, and together they depict the observatory as of 2011. Filled circles show background seismicity from 01/01/1970–13/11/2007 colored according to depth [Engdahl *et al.*, 1998]. Historical earthquake rupture regions are sketched as ellipses, rupture region of the M8.4 2001 Arequipa earthquake is outlined by the 2 m slip contour [Pritchard *et al.*, 2007], of the M8.1 Antofagasta earthquake by the 1 m slip contour [Chlieh *et al.*, 2004]; the 1 m slip contour of the M7.7 2007 Tocopilla earthquake is from this study. The black box is the extent of the map in Figure 2. Plate convergence velocity from Angermann *et al.* [1999]. MP – Meji llones Peninsula.

been thought to be aseismic. Finally, the great M9 2011 Tohoku-Oki earthquake broke a region that was not an expected seismic gap at a surprisingly shallow level in the seismogenic zone [Simons *et al.*, 2011]. Obviously, understanding subduction zone segmentation, which ultimately determines size, location and tsunami potential of subduction earthquakes, is one of the most important tasks in understanding subduction earthquake risk. While understanding of these patterns is still at an early stage because of the paucity of high resolution data, complementary numerical modeling studies [e.g., Kaneko *et al.*, 2010] have shown that rupture arrest and overlap strongly hinge on the degree of pre-stress present in the seismogenic zone

independent of lateral variability of mechanical properties or other reasons.

[3] To the west of the South American plate, convergence of approximately 6.7 cm/a with the oceanic Nazca plate is mostly accommodated by recurrent rupture of large segments of the interface between the two plates. The resultant earthquakes are among the largest and, for their sizes, most frequent on Earth. Along the Chilean and southern Peruvian margin, all segments for which there exist historic and/or instrumental records, have ruptured at least once in the past 150 years. After rupture of the Constitución gap in south-central Chile in February 2010, the segment that is considered to be most mature for re-rupture stretches for more than 500 km along the northernmost Chilean coast between roughly 23°S and 18°S [Comte and Pardo, 1991; Kelleher, 1972] (Figure 1). The entire segment broke last in 1877 in a great $M > 8.5$ earthquake [Comte and Pardo, 1991]. The segment to the north had broken nine years before in 1868 in an earthquake of similar size and partly broke again in 2001 in the M_w 8.4 Arequipa earthquake (Figure 1). The contiguous segment to the south of the 1877 rupture region was broken in 1995 by the M_w 8.1 Antofagasta earthquake that started on the Meji llones Peninsula (MP) and broke unilaterally southwards [Delouis *et al.*, 1997] (Figure 1). In November 2007 a magnitude M_w 7.7 earthquake occurred in the southern part of the seismic gap between the coastal town of Tocopilla and MP, hereinafter called Tocopilla earthquake. It is the largest event to occur within the gap left behind by the 1877 event. The 2007 main shock has been studied before using both seismic and geodetic data [Béjar-Pizarro *et al.*, 2010; Delouis *et al.*, 2009; Loveless *et al.*, 2010; Motagh *et al.*, 2010; Peyrat *et al.*, 2010]. These studies give a consistent picture to a first order showing that slip was confined to a narrow band stretching for approximately 130 km between depths of about 30–55 km and hence filling only a minor part of the seismic gap. The question arises why the earthquake did not develop into the great one that was expected here, but stopped where it did. We locate six months background seismicity preceding and about 1000 aftershocks within the first week following the main shock utilizing a permanent seismic network in the region. We determine moment tensors for the 38 largest aftershocks by modeling complete local and regional broadband waveforms. Further, we use the most complete data set to date on co-seismic static deformation from both space geodesy and near-field seismographs to derive a distributed slip model that is based on the same layered earth model that was used for earthquake location and a slab geometry derived from the aftershock plane. We relate the positions of the aftershocks to the modeled main shock slip and juxtapose our findings with earlier work on the adjoining 1995 Antofagasta earthquake to illuminate the nature of their common boundary and infer some local and also more general aspects of South American subduction fault segmentation.

2. Data

[4] We use mainly data from the Integrated Plate Boundary Observatory Chile for our analysis (IPOC, www.ipoc-network.org). IPOC is an initiative of the German Research Centre for Geosciences-GFZ, the Institute Physique

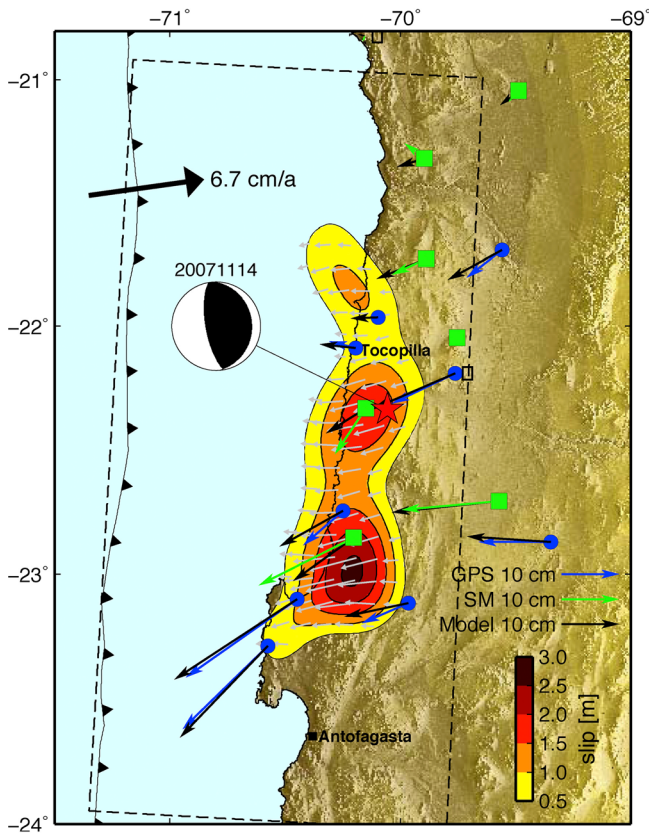


Figure 2. Slip model of the Tocopilla earthquake from inversion of static surface displacement data. Small gray arrows indicate fault slip directions on the fault plane scaled by slip amplitude. Colored vectors are observed horizontal displacement (blue: GPS, green: seismic strong motion – SM). Black vectors are horizontal displacements predicted by the depicted slip model. The dashed box is the surface projection of the 20° dipping fault plane assumed in the model. The beach ball is the stereographic lower hemisphere projection of the double-couple of the global CMT project centroid moment tensor, and the red star locates the epicenter derived in this study.

du Globe Paris, Universidad de Chile, Santiago and Universidad Católica del Norte, Antofagasta, to continuously monitor seismicity and deformation in the northern Chile seismic gap. Implementation of IPOC started in 2006 with the deployment of a backbone seismic network. At the time of the Tocopilla earthquake, twelve sites were already deployed with Streckeisen STS-2 broadband sensors and co-located strong motion accelerometers (Kinematics EPI Sensors or Güralp CMG5). IPOC sites are built at remote locations into bedrock caverns to ensure stable conditions for the measurements. As of 2011 the backbone network has expanded to 19 sites (Figure 1), including co-located continuous GPS measurements and near real-time data transmission to the GEOFON data host at GFZ (geofon.gfz-potsdam.de) at most sites. For the Tocopilla earthquake analysis we use both strong and weak motion channels from the seven sites closest to the rupture region (PB01-PB07) and the IRIS/GEOFON station LVC (Figure 1). Three of the

stations were on top of the rupture plane, whereas the other four were in its vicinity (Figures 1 and 2).

3. The Main Shock

[5] The centroid moment tensor double couple of the main shock shows a pure thrust mechanism on a shallowly dipping plane with the rake vector parallel to plate convergence (www.globalcmt.org, event ID 200711141540A, strike 358° , dip 20° , slip 98° ; Figure 2). The source rupture propagated with about 2.8 km/s and lasted for about 40 s based on kinematic inversions of seismic data [Delouis *et al.*, 2009; Peyrat *et al.*, 2010]. To derive a finite fault model with distributed slip, we inverted static surface displacement data from InSAR, GPS and double-integrated strong motion data. The InSAR line-of-sight (LOS) displacement data set stems from three passes of the ENVISAT satellite and is described in detail by Motagh *et al.* [2010]. It is of particularly high quality because the largest part of the rupture occurred beneath hyper arid land. The eleven three component GPS measurements (Figure 2) were processed and published by Béjar-Pizarro *et al.* [2010]. We derived additional three component static displacements from strong motion accelerograms recorded at IPOC sites by applying a new correction algorithm [Wang *et al.*, 2011] to remove instrumental or tilt induced baseline shifts affecting accelerograms during strong shaking that, if not properly corrected, otherwise prevent extraction of static displacement through integration. Wang *et al.* [2011] showed that static displacement derived in this way is robust, albeit of lower precision than GPS data. We accounted for the different uncertainties and number of measurements of the three data sets by giving them different weights in the inversion (Table 1). We used a rectangular fault plane of 350×180 km dimension that is aligned with the strike of the trench (Figure 2). The dip of the plane was assumed to be 20° based on the cross-section of aftershock hypocenters of this study and another study to the south [Nippres and Rietbrock, 2007] and refraction seismic experiments [Buske *et al.*, 2002; von Huene and Ranero, 2003]. The fault plane was represented by 630 discrete dislocation patches, each being 10×10 km. The surface deformation caused by each source patch was calculated using dislocation theory applied to a layered elastic earth model [Wang *et al.*, 2003]. The layer model is based on the minimum 1D seismic velocity model derived by Husen *et al.* [1999] from the aftershock data set of the neighboring Antofagasta earthquake. The same velocity model was also used to locate earthquakes and calculate moment tensors in this study. Smoothing was optimized so that the RMS stress drop from all patches is reasonable

Table 1. Data Weighting and Misfit for Distributed Slip Inversion

	E	N	Z	LOS
	<i>Weighting</i>			
GPS	40	40	20	N/A
SM	10	10	10	N/A
InSAR	N/A	N/A	N/A	1
	<i>RMS Misfit (cm)</i>			
GPS	2.6	0.8	1.3	N/A
SM	2.3	1.9	2.1	N/A
InSAR	N/A	N/A	N/A	1.0

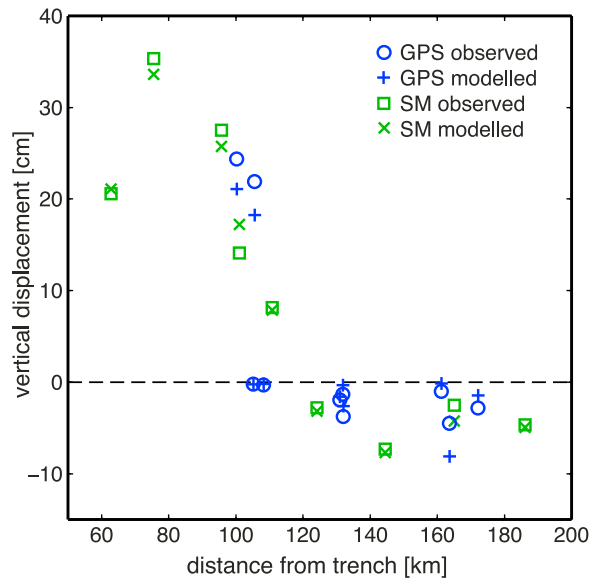


Figure 3. Observed GPS and seismic strong motion (SM) and modeled vertical static displacement.

(approximately 0.8 MPa for the shown model) and the misfit is acceptable. Misfit for the three data sets and components is tabulated in Table 1.

[6] The moment magnitude of the slip model is $M_w = 7.83$, which is somewhat larger than the $M_w = 7.7$ obtained by the global CMT project. The higher moment can probably be attributed to both some unconstrained slip on the edges of the model and post-seismic deformation that is included in particular in the InSAR data set.

[7] Figure 2 shows the slip map (Data Set S1 of the auxiliary material) and observed and modeled horizontal displacements from GPS and seismic strong motion, and Figure 3 shows observed and modeled vertical displacements.¹ Rupture was confined to an approximately 130×75 km swath that roughly parallels the coastline.

[8] Slip spans a depth range of 30–55 km and thus only the deepest part of the seismogenic zone, where the plates are coupled and inter-plate thrust earthquakes occur. The slip distribution shows two patches, with one near the hypocenter and one further south. Maximum slip was 2.6 m on the southern patch. The earthquake terminated in the south in the center of the MP. The rupture limits and size and location of the two asperities are in very good agreement with various published slip maps based on geodetic data only [Béjar-Pizarro *et al.*, 2010; Motagh *et al.*, 2010], teleseismic data, near-field strong motion data [Peyrat *et al.*, 2010] and a combination [Delouis *et al.*, 2009; Loveless *et al.*, 2010] using various model parameterizations, data weighting, geometries and regularizations etc., corroborating the main features of the model presented in this study.

4. Pre-Main Shock Seismicity and Aftershock Sequence

[9] We relocated 6 months of pre-main shock seismicity and aftershocks that occurred in the week following the main

shock. This amounts to 1108 events with local magnitude $M_l > 1.5$ (Data Set S2 of the auxiliary material). The catalog appears to be complete at approximately $M_l = 2.7$ based on a magnitude-frequency histogram. We used hand-picked arrival times for initial single-event locations (HYPO71 [Lee and Lahr, 1975]), and a joint hypocenter determination (JHD) algorithm (VELEST [Kissling *et al.*, 1994]) for a first relocation. We took advantage of the robustness of the JHD locations to weed out spurious phase picks. We then derived cross-correlation based differential travel times and used the double-difference algorithm [Waldhauser and Ellsworth, 2000] to further refine the locations. All (re)location steps were taken using the minimum 1D velocity model of Husen *et al.* [1999]. To obtain differential travel times, we windowed the vertical component from 0.5 s before to 1.5 s after the *P* pick and the two horizontal components from 1.0 s before to 2.0 s after the *S* pick. We integrated the horizontal traces containing the *S* phase to displacement before cross-correlation because we found that this enhances the *S* signal. A 3-pole causal 1–10 Hz Butterworth band-pass filter was applied to all waveforms. We calculated the cross-correlation function for event pairs with a maximum epicentral separation of 15 km. For the *S* phase windows, we stacked the cross-correlation function of the two horizontal components and obtained the lag time and correlation coefficient from the maximum amplitude of the stack. Lag times with a correlation coefficient >0.7 were kept and furnished with the correlation coefficient as a weight for the hypocenter inversion. This procedure yielded 15,350 lag time measurements. We found similar waveforms mainly for the three stations closest to the aftershock cloud (PB04, PB05, PB06) because they exhibit rather simple, impulsive arrivals. The stations that were further away often showed emergent and complex waveforms, probably due to phases traveling along the high velocity slab and multipathing.

[10] Figure 4 shows views of seismicity during six months preceding the main shock and 24 h and 7 days following the main shock. Pre-main shock background seismicity occurs mainly north of 22°S and along a narrow band between the updip limit of the main shock and the coastline. The region further seaward and south of the rupture was virtually aseismic. It should be noted, however, that the detection capability diminishes southward due to the lack of stations. The southern main shock asperity shows very little pre-main shock seismicity. Three small earthquakes preceded the main shock by 48 h. These comprise a $M_l 3.6$ (42 h before main shock), a $M_l 1.9$ (30 h before main shock) just updip of the main shock hypocenter, near the coastline, and a $M_l 3.3$ (34 h before main shock) just north of MP (Figure 4). The E-W cross-section reveals that the earthquakes preceding the Tocopilla earthquake formed an eastward dipping seismogenic zone. There was hardly any upper plate seismic activity.

[11] During the first 24 h following the main shock, the seismicity distribution is in very good agreement with the region that slipped during the earthquake, with the southern asperity of highest slip being mostly void of aftershocks. We notice that aftershocks align along the coastline on the northern Mejillones Peninsula and also south of the coastal town of Tocopilla. There were only a few stray earthquakes clearly seaward of the main shock rupture. After approximately 24 h two large aftershocks (2007-11-15 15:03 $M_w 6.3$ and 2007-11-15 15:05 $M_w 6.8$) occurred at the northwestern

¹Auxiliary materials are available at <ftp://ftp.agu.org/apend/jb/2011/jb009030>.

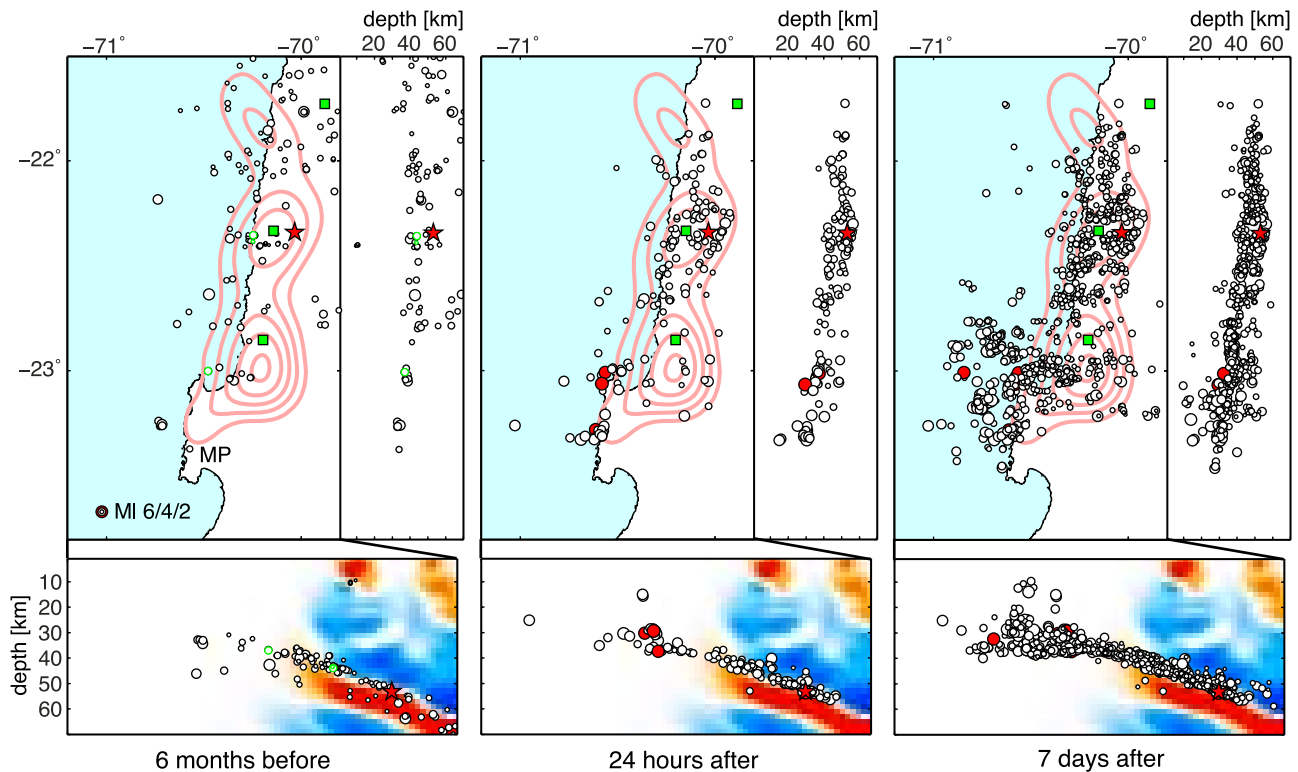


Figure 4. Relocated seismicity maps and cross-sections for the time periods 6 months before and 24 h and 7 days after the 11/14/2007 main shock. The three events marked green occurred within 42 h before the main shock. 0.5 m slip contour lines and main shock epicenter are also plotted. The EW cross-section shows in the background receiver functions of *Sodoudi et al.* [2011] that we migrated using *Husen et al.*'s [2000] velocity model; the red (positive conversion amplitude), eastward dipping structure is due to the phase conversion along the oceanic Moho discontinuity. Red filled circles have magnitudes $M_I > 6$. Green squares are stations used in the analysis. MP – Mejillones Peninsula.

tip of MP (Figure 4, middle). These events marked the origin in space and time of a band of seismicity propagating in an arc northeast and east and downdip into the – until then – aseismic region of the southern slip asperity. This event cluster remained extremely active, producing small earthquakes continuously during the remaining observation period. Other than these, aftershocks spread mainly seaward west and northwest of MP in the following days. This offshore area accumulated the highest post-seismic moment release during our analysis period (Figure 5b). The same region was aseismic in the six months preceding the earthquake.

[12] In Figure 5a we plot normalized aftershock density and main shock slip for comparison. For the northern part of the rupture region there is a striking congruence of the two measurements, i.e., high seismicity on the northern asperity and low seismicity outside the area that slipped and in the region between the two asperities. In the south, main shock slip and earthquake density are rather anti-correlated with the southern asperity remaining relatively aseismic but for the cluster related to the 2007-11-15 events mentioned above, and a high density of aftershocks updip of the slip region. The southern rupture limit is sharply defined across and just north of the center of the MP for both slip and aftershock activity.

[13] Despite the sparseness of the network, the aftershocks sharply define a thin plane in the east-west cross-sections (Figure 4). We used receiver functions processed by *Sodoudi et al.* [2011] to image the subducting plate. Receiver functions were migrated using the velocity model of *Husen et al.* [2000] that was also used for location (Figure 4). The center of the eastward dipping red (positive) converted phase is most likely caused by the high-to-low (in the direction of the teleseismic ray) velocity contrast at the oceanic Moho. The narrow band of the projected seismicity locates approximately 10 km above the oceanic Moho. This suggests that the events occurred on the thin shear zone between the two plates.

[14] The downdip limit of seismicity is at about 55–60 km depth, deepening to the north. The only earthquakes possibly occurring in the upper plate are offshore, where the network geometry gives limited depth resolution, and hence caution should be exercised when interpreting them.

5. Moment-Tensor Inversion of Aftershocks

[15] We determined fault mechanisms and centroid depths for 38 aftershocks through moment tensor inversion (Table 2 and Data Set S3 of the auxiliary material). We modeled only the strongest aftershocks for which the signal at long periods

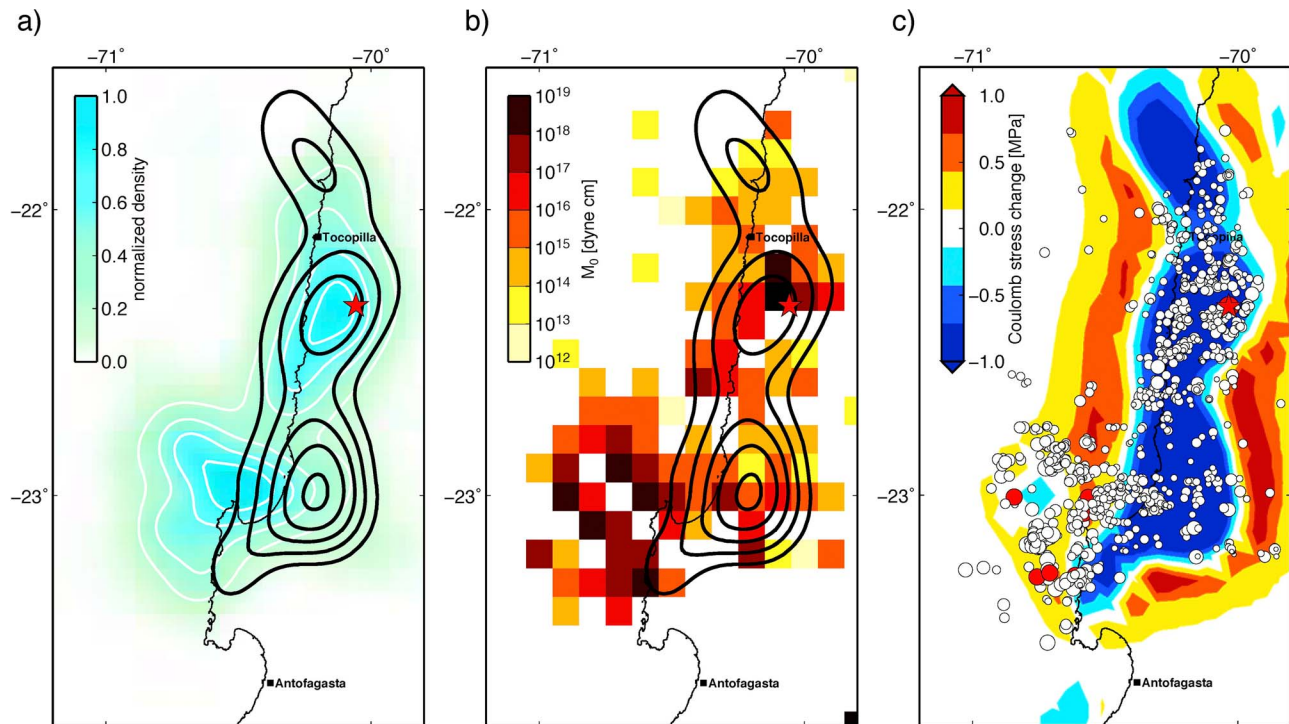


Figure 5. (a) Normalized Gaussian kernel earthquake density for the seven days of aftershocks plotted in Figure 4c. The 0.5 m main shock slip contour lines and main shock epicenter are also plotted here and in Figure 5b. (b) Cumulative seismic moment for the same seven days of aftershocks assuming the hypocenter as the centroid point source. (c) Coulomb stress change due to the main shock slip (see Figure 2) on the same 20° east dipping reverse fault plane used for slip inversion.

(>10 s) was sufficient (M_w from 3.9 to 6.8). Seismograms from events within the first 12 h were contaminated by persistent long-period ground disturbance following the main rupture and countless aftershocks, preventing determination of fault plane solutions in this period. We modeled complete regional three component displacement seismograms from IPOC stations and the IRIS/Geofon station LVC at long periods (Figure 6a). Green's functions were calculated for the layered 1D model that was also used for hypocenter location using a discrete wave number summation method that includes near-field terms [Bouchon, 1981]. The inversion was done in the time domain applying a deviatoric constraint to the moment tensor [Nábělek and Xia, 1995]. Although the stations cover only a quarter of the focal sphere for most events, the consistency of the mechanisms gives us confidence in the robustness of the results. Thirteen of the 38 modeled events also have moment tensors from the global CMT project and the median deviations for the nodal plane parameters between the two sets of solutions are 10° for strike, 6° for dip and 13° for rake. The majority of the events have a mechanism that is similar to the main shock, i.e., involving a north by west striking and east dipping low-angle thrust plane (Figure 7), suggesting that most of the larger aftershocks ruptured on the megathrust. Most events of this category occur in clusters offshore west and northwest of MP, where there is little to no co-seismic slip, but where post-seismic moment release is highest (Figure 5b) and where Béjar-Pizarro *et al.* [2010] observed some afterslip (Figure 8). A few events show dip-slip mechanisms involving one steep or near vertical nodal plane

(e.g., Figure 7). To obtain better constraints for the depths of the offshore events we used waveform modeling. We determined depth by observing the data fit for a suite of trial depths (Figure 6b) in our moment tensor inversion routine. Hypocentral depth versus the centroid depth derived in this manner is graphed in Figure 6c and a cross-section is plotted in Figure 7. In the cross-section the centroid depths form an east-dipping plane, giving us confidence in the general capability of the long-period seismograms to resolve depth. Hypocentral and centroid depths correlate, but there is significant scatter and centroid depths are generally shallower for the western, offshore events (Figures 6c and 7). We observe a group of events, however, that clearly locates above the dipping plane. These events are colored blue in Figures 6c and 7. They also exhibit different mechanisms compared to the main shock and the majority of aftershocks that fall on the dipping plane, i.e., thrusts with slightly rotated strikes and also dip-slip mechanisms involving one steep or near vertical nodal plane (e.g., Figure 6). We believe that they occurred in the upper plate and hence not all of the apparent broadening of the seismogenic zone can be attributed to errors in depth. These upper plate events all occur in clusters just west of MP. In comparison, the events further north, offshore and also the deeper ones within the co-seismic rupture region appear to involve only the megathrust plane. The two largest events we modeled are the two events occurring within three minutes approximately 24 h after the main shock (2007-11-15 15:03 M_w 6.3 and 2007-11-15 15:05 M_w 6.8, Table 2). They occurred close together at the northwestern tip of MP (see also Figure 4

Table 2. Source Parameters From Double Couple Component of the Inverted Moment Tensor for 38 Large Aftershocks

Latitude (deg)	Longitude (deg)	Hypocentral Depth (km)	Centroid Depth (km)	Date	Time	M_0 (dyn cm)	M_w	Nodal Plane 1			Nodal Plane 2		
								Strike (deg)	Dip (deg)	Rake (deg)	Strike (deg)	Dip (deg)	Rake (deg)
-23.326	-70.688	30.4	27.0	2007/11/15	01:46:34.78	1.16e+24	5.34	184	68	98	344	23	71
-22.312	-70.331	42.0	33.0	2007/11/15	03:25:13.81	1.71e+22	4.12	162	65	86	351	25	97
-23.310	-70.579	29.6	27.0	2007/11/15	03:27:26.96	2.38e+22	4.21	174	68	87	1	22	96
-22.336	-69.963	55.8	51.0	2007/11/15	04:29:53.60	5.04e+22	4.43	171	66	78	18	26	115
-22.099	-70.208	46.3	36.0	2007/11/15	07:07:09.10	1.43e+22	4.07	174	73	69	46	27	139
-23.310	-70.667	31.4	24.0	2007/11/15	09:31:27.47	5.92e+22	4.48	182	68	96	346	23	75
-23.260	-71.027	25.2	21.0	2007/11/15	11:14:45.43	7.17e+23	5.20	175	59	98	338	32	76
-23.009	-70.564	37.3	33.0	2007/11/15	15:03:06.40	3.18e+25	6.30	180	70	97	342	21	73
-23.062	-70.581	29.4	24.0	2007/11/15	15:05:56.38	1.75e+26	6.79	179	71	106	318	25	51
-23.003	-70.429	38.2	30.0	2007/11/15	21:05:33.12	4.23e+22	4.38	167	58	79	6	34	106
-22.935	-70.891	36.3	21.0	2007/11/15	21:12:20.59	3.90e+23	5.02	181	62	98	343	29	74
-22.991	-70.489	37.7	27.0	2007/11/16	01:53:05.21	5.28e+22	4.45	171	68	98	331	24	72
-22.583	-70.020	52.6	51.0	2007/11/16	05:56:41.09	1.00e+22	3.96	181	73	101	328	20	58
-22.930	-70.572	37.2	24.0	2007/11/16	08:42:38.64	1.67e+24	5.45	173	67	92	348	23	85
-23.295	-70.643	30.4	27.0	2007/11/16	14:34:05.15	6.72e+23	5.18	186	70	104	330	24	56
-22.179	-70.033	53.1	54.0	2007/11/16	17:05:19.84	3.07e+23	4.95	170	65	88	355	25	95
-22.816	-70.573	35.9	21.0	2007/11/16	19:07:24.23	5.12e+22	4.44	161	62	79	4	30	110
-23.290	-70.735	31.8	9.0	2007/11/16	21:09:30.69	1.92e+23	4.82	171	89	84	72	6	170
-23.026	-70.310	39.5	36.0	2007/11/17	03:07:31.33	1.69e+24	5.45	168	66	89	351	24	92
-22.550	-70.298	42.0	36.0	2007/11/17	03:20:14.21	2.78e+22	4.26	167	69	83	6	22	108
-23.173	-70.795	28.6	18.0	2007/11/17	17:54:31.41	9.73e+24	5.96	196	85	109	300	20	15
-23.178	-70.776	29.9	15.0	2007/11/17	18:13:13.32	1.07e+24	5.32	207	78	99	350	16	54
-23.184	-70.745	28.9	12.0	2007/11/17	19:25:43.27	1.84e+23	4.81	23	73	-117	263	32	-34
-23.165	-70.755	31.4	12.0	2007/11/17	19:59:19.73	6.51e+22	4.51	356	78	-86	156	13	-110
-23.179	-70.749	29.8	15.0	2007/11/17	22:17:28.76	3.86e+23	5.02	192	72	93	2	18	81
-23.138	-70.699	28.9	18.0	2007/11/18	12:15:36.97	3.96e+24	5.69	184	68	114	314	32	44
-22.824	-70.755	37.3	21.0	2007/11/18	15:24:53.21	3.14e+23	4.96	164	66	92	339	24	86
-22.912	-70.702	38.2	24.0	2007/11/19	18:19:19.45	3.92e+23	5.03	178	67	97	340	24	74
-22.003	-70.298	44.4	30.0	2007/11/19	18:46:12.94	6.67e+21	3.85	167	76	94	330	15	74
-22.896	-70.679	38.0	24.0	2007/11/19	20:21:08.48	9.20e+23	5.27	179	65	98	341	26	74
-22.906	-70.724	36.7	21.0	2007/11/19	23:30:28.47	8.13e+24	5.90	180	67	99	337	25	69
-23.116	-70.166	42.1	42.0	2007/11/20	00:51:09.51	2.06e+23	4.84	161	73	84	1	18	109
-22.886	-70.876	36.0	15.0	2007/11/20	01:24:49.58	1.83e+23	4.80	179	62	98	344	28	76
-22.887	-70.679	37.8	21.0	2007/11/20	04:56:15.56	2.05e+23	4.84	178	69	91	357	22	88
-22.873	-70.693	38.6	24.0	2007/11/20	06:41:06.99	1.79e+23	4.80	177	67	94	348	23	81
-23.226	-70.718	14.0	21.0	2007/11/20	16:44:28.72	1.54e+24	5.42	189	69	97	350	22	73
-23.007	-70.843	32.4	24.0	2007/11/20	17:55:48.50	1.59e+25	6.10	182	65	102	335	28	66
-22.949	-70.629	36.8	24.0	2007/11/20	22:38:30.43	8.81e+22	4.59	184	68	101	336	24	65

middle panel). Travel time based hypocentral depths differ by eight kilometers with the second, larger event being shallower. This depth difference is corroborated by waveform modeling (nine kilometers difference). Both events have nearby epicenters, similar mechanisms and very good signal-to-noise ratios. Hence, the vertical separation cannot be attributed to path effects or noise contaminating waveforms or travel times, but is probably real, possibly indicating either activation of a splay fault above the megathrust or a generally less localized shear zone here. We also note that the apparent widening of the seismogenic zone begins sharply at the western limit of MP.

6. Discussion

6.1. Co-seismic Slip Versus Aftershock Pattern

[16] The Tocopilla earthquake ruptured only a piece of the deepest part of the seismogenic zone along a narrow swath with its updip limit roughly paralleling the coastline just offshore. The rupture region is congruent with the aftershock region during the earliest part of the sequence. Later, the aftershocks propagated offshore, but only off the southern part of the rupture, west and northwest of MP. In the

northern part, aftershocks remained confined to the co-seismic rupture area. In order to better understand the aftershock pattern with respect to the main shock slip, we modeled the stresses imparted by the main shock on the same 20° dipping plane (assuming reverse slip, i.e., a rake angle of 90°) that was used for modeling main shock slip. This choice seems justified, because the aftershock hypocenters and source mechanisms suggest that the majority of the aftershocks are related to the plate interface. We used the software Coulomb 3.2 [Lin and Stein, 2004; Toda et al., 2005] and similar model parameters as Lin and Stein [2004] used for modeling the neighboring Antofagasta earthquake, i.e., Young's modulus $E = 8 \times 10^4$ MPa, Poisson's ratio $\sigma = 0.25$, but a lower effective coefficient of friction more suitable for northern Chile, i.e., $\mu = 0.1$ [Lamb, 2006]. The surface projection of the static Coulomb stress changes on the fault plane is mapped in Figure 5c. The pattern is essentially such that Coulomb stress is decreased where the fault slipped and increased on the rupture's fringes. In the northern part of the fault there is a clear anti-correlation between Coulomb stress increase and aftershock density (Figures 5a and 5c). In the southern part of the fault, aftershocks cluster above the updip end of rupture, where a significant boost in Coulomb stress

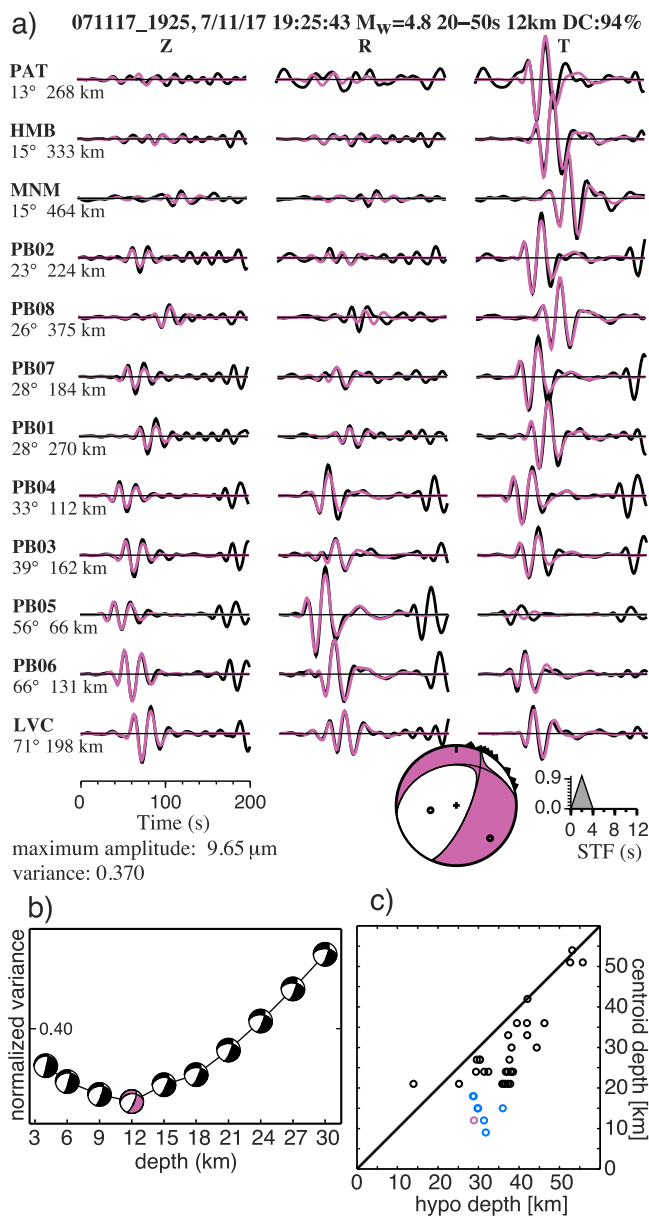


Figure 6. Moment tensor inversion for a moderate aftershock. (a) Observed (black) and modeled (purple) complete long-period regional seismograms. Azimuth and distance is noted below the station codes. The phase, which is not modeled in the late part of the time series, is from a second event. The mechanism of the event is extensional and significantly different from those of most of the other modeled aftershocks. The beach ball is marked in the same purple color in the map and cross section of Figure 7. (b) Variance versus depth for the event. Best fit is achieved at 12 km depth, placing the event in the upper plate. (c) Hypocentral depth from standard travel time based hypocentral inversion versus centroid depth from waveform modeling. Although there is a clear correlation between the two depths, centroid depths are generally shallower than hypocentral depths. Hypocentral depths offshore are hampered by unfavorable event-station geometry. Blue and purple events have centroid depths ≤ 18 km and are presumably located in the upper plate. They are marked in the same color in Figure 7.

is predicted. Here we also find the largest events and highest post-seismic moment release (Figure 5b), including several events with $M > 6$, as well as some slow afterslip (Figure 8) [Béjar-Pizarro *et al.*, 2010]. The almost complete absence of aftershocks updip of the northern part of the rupture, where Coulomb stress has been increased by several tenths of MPa, is conspicuous. This part of the subduction zone was totally locked before the 2007 Tocopilla earthquake [Chlieh *et al.*, 2004; Khazaradze and Klotz, 2003] and, obviously, it did not yield despite loading from the contiguous slip. Béjar-Pizarro *et al.* [2010] suggested that a kink in the subducted slab could be responsible for inhibiting rupture to propagate updip. Such a kink has been suggested earlier by Armijo and Thiele [1990] to explain large-scale tectonics of

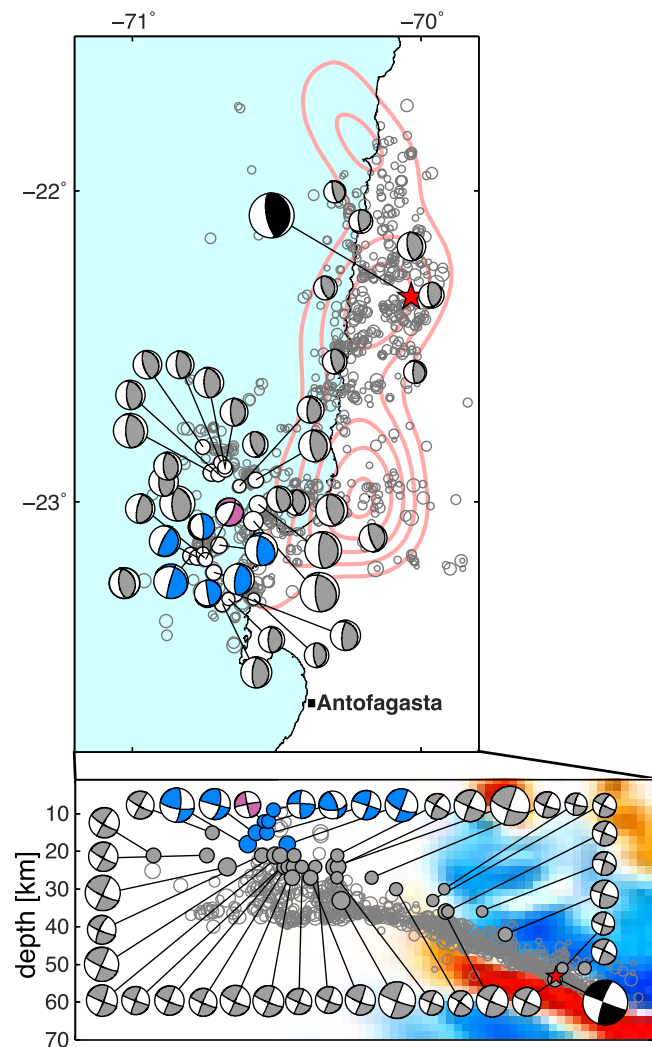


Figure 7. Beach balls depicting the double-couple component of the moment tensors. The main shock (black) is from global CMT project, the aftershocks (gray/blue/purple) from this study. Most of the aftershocks have a mechanism similar to the main shock, i.e., east of north striking shallow thrust. Waveforms of event marked purple are shown in Figure 6. Modeled events in cross section point to centroid depth. Events with centroid depths ≤ 18 km are marked in blue. These events have mechanisms that differ from the main shock thrust and occurred presumably in the upper plate.

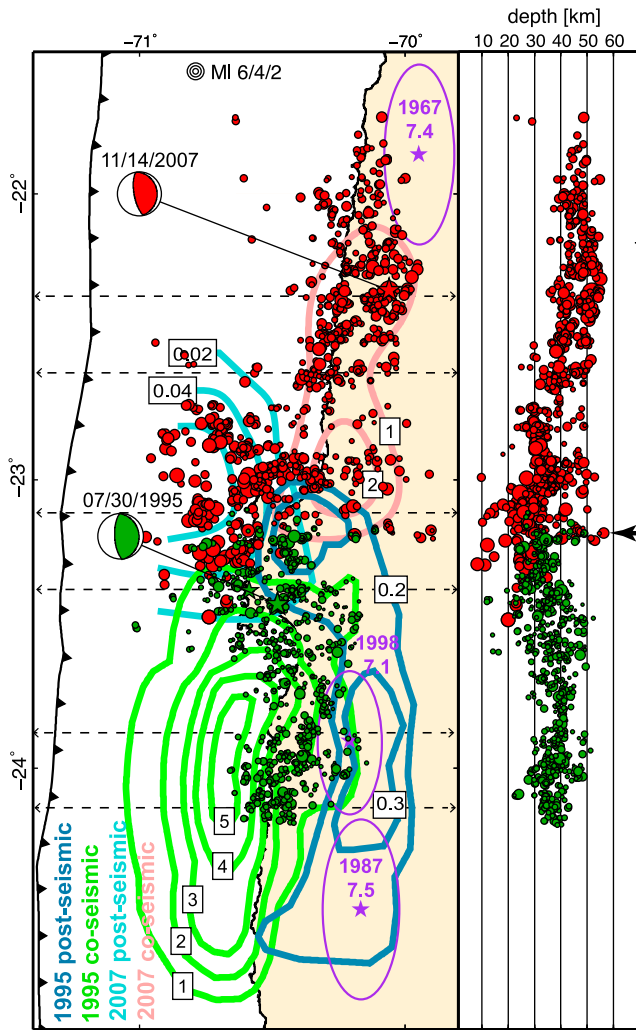


Figure 8. Slip and aftershocks of the M8.1 1995 Antofagasta and M7.7 2007 Tocopilla earthquakes. Green circles are relocated aftershocks of the Antofagasta event [Nippres and Rietbrock, 2007]. Slip and net aseismic afterslip of the Antofagasta event are from Chlieh et al. [2004], afterslip for the Tocopilla event from Béjar-Pizarro et al. [2010]. The values in the boxes are in meters. The epicenters of the main shocks are shown as stars. Three events with $M > 7$ are also plotted [Malgrange and Madariaga, 1983; Pritchard et al., 2006]. The dashed lines mark the corridors for projected seismicity in the cross sections in Figure 9. Small black arrow points to a lineament of events discussed in the text.

the northern Chilean coastal forearc. A change in dip, however, is not perceptible in the northern and southern cross-sections and in fact the slab has to be continued quite straight at 20° dip in order to top out near the trench (Figure 9). A kink in the slab would also cause deformation and stress concentration in the hanging wall. Above such a kink one would expect earthquakes in the upper plate, but such a feature is not visible in at least the northern cross-section (Figure 9).

[17] We speculate that the pattern of co-seismic slip, post-seismic slip and aftershocks reflects different frictional

properties of the inter-plate fault plane varying both down-dip and along strike. We base the following discussion on the principles of rate-and-state dependent friction theory [e.g., Scholz, 1998, and references therein]. Accordingly, three frictional regimes exist, namely “unstable,” “conditionally stable” and “stable.” Unstable slip results in excitation of seismic waves while stable slip is regarded as aseismic. “Unstable” slip is generally attributed to intrinsic velocity weakening, that is, frictional strength decreases with increasing slip velocity. Using the “steady state” approximation, i.e., discarding transient phases associated with changes in slip velocity, velocity weakening behavior is characterized by a negative difference between the absolute values of the parameters a and b describing the direct (rate) and evolutionary (state) effects on frictional strength, respectively, following a velocity change, i.e., $a - b < 0$. Below a critical normal load, slip on an intrinsically velocity weakening interface may be “conditionally” stable, that is aseismic until an external acceleration triggers a slip instability to occur. The acceleration needed to trigger seismic failure depends inversely on normal load. The latter might not only be controlled by overburden but also by pore fluid pressure. Finally, in the “stable” regime, only aseismic creep occurs controlled by a velocity strengthening behavior (that is frictional strength increases with slip velocity, $a - b > 0$).

[18] A key observation in the study area is that aftershocks occur in the Tocopilla rupture area despite a predicted Coulomb stress decrease here (Figure 5c). This counter intuitive observation may be attributed to (A) a more heterogeneous rupture than is suggested by the smooth slip inversion models, leaving behind a small scale mosaic of remnant, positively stressed patches that break post-seismically [e.g., Helmstetter and Shaw, 2006] or (B) reloading of the main shock area by afterslip [e.g., Helmstetter and Shaw, 2009]. For the Tocopilla earthquake no afterslip is detected within the main shock slip area, favoring the idea of small-scale heterogeneities in co-seismic slip and the remnant stress fields. If so, does the Tocopilla aftershock activity reflect frictional properties that are heterogeneous at small scale and what are their causes? A regularly sketched model of the subduction seismogenic zone is that the plate interface is paved with seismic and aseismic patches of varying size [e.g., Bilek and Lay, 2002; Schwartz and Rokosky, 2007]. Large seismic (velocity-weakening) areas are thought to represent asperities that accumulate stress in the inter-seismic period and break in large earthquakes. Smaller patches may accumulate less stress and break more often in smaller earthquakes. The underlying nature of the variation in frictional behavior, however, is unclear. Assuming that the rate-state parameters a and b are rather persistent material properties controlled by temperature, pressure and mineralogy, i.e., controlling factors that change at large scale and dominantly in the dip direction in a subduction zone, a viable mechanism to change frictional slip stability at small scale both in the dip direction and along strike in the subduction zone as well as in time seems to be pore fluid pressure. Recalling the rate-state theory, we argue that the aftershock region is therefore at least partially and/or temporally characterized by the “conditionally stable” regime which may slip both in an unstable (seismic) or a stable manner (aseismic) controlled solely by the ratio of deformation rate to pore fluid pressure. Accordingly, areas

of high pore fluid pressure (fluid pockets) may have resisted instantaneous co-seismic rupture because the ratio of deformation rate/pore fluid pressure was locally not high enough to trigger instability. Post-seismically, a damage induced increase in permeability may then have allowed fluid to drain from these pockets, thus favoring their delayed failure by raising the deformation rate/fluid pressure ratio and shifting the system into the unstable regime.

[19] This mechanism agrees with a model of inter-seismic locking of northern Chile that requires a kinematic transition zone where inter-seismic slip tapers from zero in the totally locked part to plate velocity between 35 and 55 km depth [Chlieh *et al.*, 2004], which is exactly the depth extent of the Tocopilla earthquake (Figure 9). Such a “partially locked” transition zone is consistent with a conditionally stable regime because inter-seismic slip is rather slow ($< =$ plate

convergence rate) and likely aseismic if assisted by moderately high pore fluid pressures. However, to nucleate a rupture like the Tocopilla earthquake in the proposed transition regime at least transiently. Updip of this transition zone, frictional properties appear to change along-strike from north to south from frictionally unstable, i.e., currently locked, no aftershocks, no afterslip, to conditionally stable, i.e., little co-seismic slip, a high number of aftershocks, afterslip northwest and west of MP.

[20] Notably, virtually no aftershocks occurred beyond the downdip end of rupture, where Coulomb stress increase would argue for triggered afterslip possibly associated with aftershocks. We believe that the downdip end of co-seismic slip, which coincides with a sharp termination of aftershock seismicity, is the downdip end of the velocity weakening

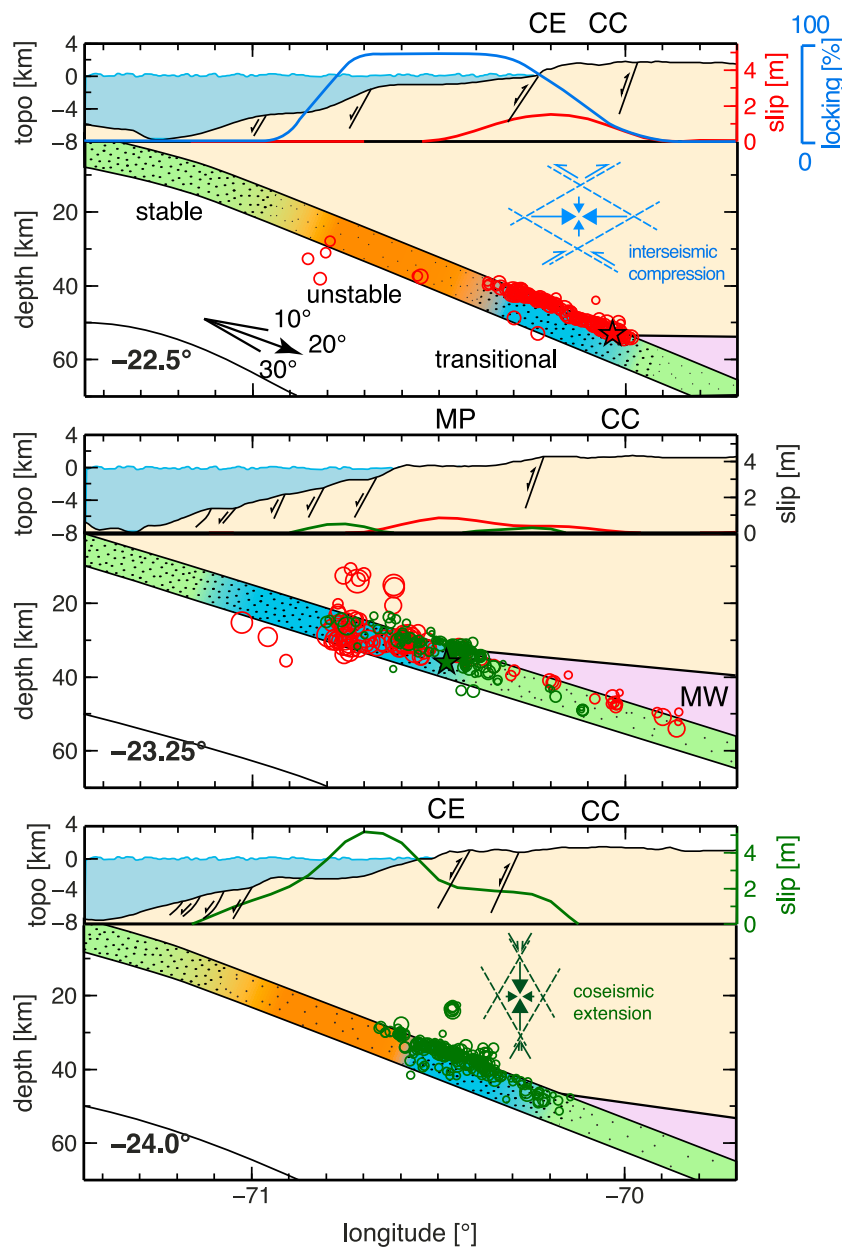


Figure 9

(integrating both unstable and conditionally stable areas) zone at large. Temperatures on top of the slab here are much lower than 350° [Oleskevich *et al.*, 1999; Springer, 1999; Wada and Wang, 2009], which represents the onset of quartz plasticity that can cause termination of seismogenic/stick-slip behavior for younger, hotter slabs. Therefore it is more likely that the subducted slab comes in contact with forearc mantle rocks characterized by more ductile, velocity strengthening deformation (i.e., serpentinite). Although there have been numerous active and passive seismic experiments in northern Chile, the exact location of the intersection of the oceanic crust with the tip of the mantle wedge is difficult to image, because the contact of serpentinitized mantle rocks with a mafic lower crust has a low impedance contrast, making it difficult to detect with seismic techniques relying on reflected or converted phases [Giese *et al.*, 1999; Sodoudi *et al.*, 2011]. Crustal thickness beneath the Coastal Cordillera is about 50 km [Bock *et al.*, 2000; Patzwahl *et al.*, 1999; Wigger *et al.*, 1994], in general agreement with the deepest slip and aftershocks. The tip of the mantle wedge in the Atacama region has been inferred to be serpentinitized based on high v_p/v_s ratios [Graeber and Asch, 1999; Schurr and Rietbrock, 2004], that would promote stable, aseismic slip. A similar depth of the downdip limit of the seismogenic zone has also been inferred by a change in the stress regime of micro-seismicity from compressional to tensile [Delouis *et al.*, 1996].

6.2. Relation to the 1995 Antofagasta Earthquake Sequence

[21] We juxtapose the 2007 Tocopilla earthquake and aftershock series with the 1995 Antofagasta earthquake that ruptured the segment just to the south to shed light on their relation and the nature of their common boundary beneath MP. We plot the 2007 Tocopilla sequence together with the 1995 Antofagasta aftershock series that was relocated based on a dense local network including ocean bottom seismometers utilizing the same velocity model as was used in our study [Nippress and Rietbrock, 2007]. Recording for this data set started approximately three weeks after the Antofagasta main shock, explaining the generally smaller

magnitudes of the events (smaller symbol sizes in Figure 8). Figure 8 reveals a striking symmetry across an axis in the center of MP, where the two sequences abut closely with virtually no overlap onshore. Overlap between the two aftershock series occurs only just seaward of MP, where events cluster along the coastline. It is remarkable that the band of aftershocks occurring on the plate interface in 30–40 km depth seems to follow the morphology of the coastline including the MP and the general trend of the coastline's increasing distance from the trench from south to north. This feature is expressed in a deepening of the seismicity on the dipping interface from south to north.

[22] The symmetry of the two sequences with respect to MP is not paralleled by a symmetry of the slip patterns, with the 1995 Antofagasta slip [Chlieh *et al.*, 2004] concentrating more updip, offshore, while the Tocopilla slip occurred more downdip, onshore. Antofagasta aftershocks, including a M7.1 event three years later, however, concentrate along the downdip region of rupture, and aseismic afterslip is focused at an even deeper level (Figure 8) [Chlieh *et al.*, 2004; Pritchard and Simons, 2006]. Antofagasta aftershocks occurred roughly in the along strike extension of the Tocopilla rupture zone. Therefore, in our view the Antofagasta band of aftershocks, just as the Tocopilla aftershock sequence, outlines the region of the plate interface with conditionally stable frictional behavior. In contrast, regions exhibiting unstable behavior, i.e., that show high slip for the Antofagasta case and locking for the Tocopilla case are post- and inter-seismically quiet. For the Antofagasta case, rupture of the unstable part of the seismogenic zone must have released stresses quite homogeneously and completely as no aftershocks occur in the rupture area, in contrast to the Tocopilla earthquake. The combination of slip and aftershock distribution also shows quite clearly that the Antofagasta rupture penetrated the transition zone in its northern half (Figures 8 and 9). The southern part of the transition zone broke earlier in 1987 in a M7.5 earthquake [Pritchard *et al.*, 2006] (Figure 8). Rupture of the 1995 Antofagasta earthquake initiated in the bay south of MP, right on the border between the unstable part of the seismogenic zone

Figure 9. Three cross-sections through aftershocks and forearc topography/bathymetry. MP – Mejillones Peninsula, CC – Coastal Cordillera, CE – Coastal Escarpment, MW – Mantle Wedge. Aftershocks are projected along a 30 km wide corridor centered on the latitude noted on the lower left corner. The cross section in the middle crosses the center of MP. Slip is shown for the Tocopilla earthquake from this study (red) and for the Antofagasta earthquake (green) [Chlieh *et al.*, 2004]. Locking of the seismogenic zone is also inferred from Chlieh *et al.* [2004]. The forearc wedge offshore MP has a continuous slope of about 5° . In contrast, north and south of MP the wedge is clearly segmented into an outer slope, a basin and an inner slope that includes the CE that forms the coastline. The basins overlie high slip or high locking. Inner slope, high locking gradient and aftershock seismicity coincide. We infer three frictional regimes: Stable (green): velocity-strengthening, earthquake-nucleation/propagation inhibited, no aftershock but afterslip, aseismic creep, variable locking. Transitional/conditionally stable (blue): velocity-weakening, earthquake-nucleation/propagation at low pore fluid pressures, small to large earthquakes with incomplete stress drops/heterogeneous remnant stress field, aftershocks/afterslip, aseismic creep/partial locking. Unstable (orange): velocity-weakening, earthquake-nucleation possible, rupture propagation sustained, great earthquakes with complete stress drop, few aftershocks/afterslip. We believe that the transition from inter-seismically fully locked to creeping of the plate interface, where it meets the mantle wedge, puts the forearc under compression and causes long-term uplift of the CC. The vectors indicate the proposed orientation of maximum and minimum principal stresses (large arrows = σ_1 and small arrows = σ_3 , respectively) at the respective stages of the seismic cycle. Following Anderson's faulting theory, horizontal σ_1 indicates the compressional regime, vertical σ_1 the extensional (normal faulting). The thinner stippled lines indicate the orientation of faults that are preferentially reactivated σ_1 bisects the acute angle between the conjugate shear fractures; σ_3 bisects the obtuse angle between the conjugate shear fractures. Half arrows indicate sense of shear.

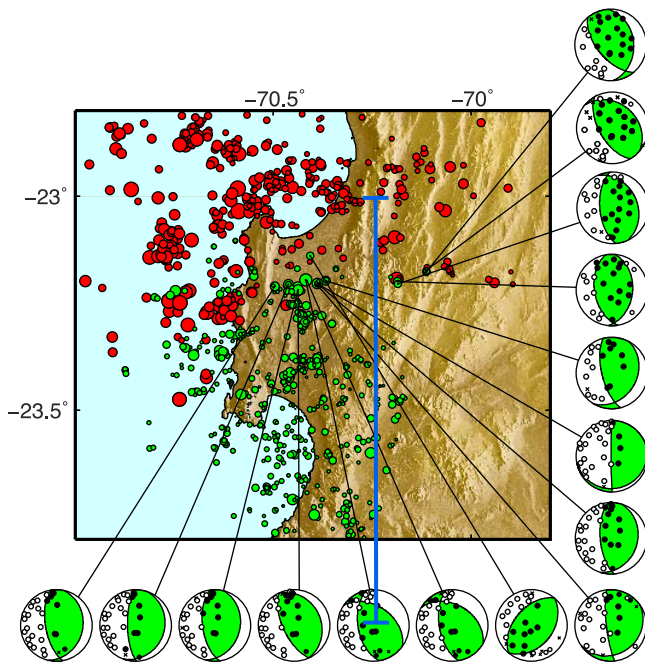


Figure 10. First motion fault plane solutions from 1995 Antofagasta aftershocks along the sharp boundary to the 2007 Tocopilla earthquake. All mechanisms are well-determined thrust types. The blue line indicates the extent of the cross section in Figure 11.

and the conditionally stable transition zone [Delouis *et al.*, 1997] (Figure 8).

6.3. Along-Strike Segmentation and the Role of Mejillones Peninsula

[23] The two earthquake sequences are separated by MP and its offshore extension. The peninsula's isolated position on an otherwise straight coastline and its perfect symmetry have raised particular curiosity about its formation and origin [Armijo and Thiele, 1990]. Based on the correlation of short- and long-term observations, it has been speculated that it serves as a "persistent" segment boundary for large earthquakes on a million year time scale [Victor *et al.*, 2011]. At least the 1995 and 2007 ruptures show an obvious spatial relationship with it. The 1877 event's southern limit was probably also close to the peninsula based on historical accounts of the earthquake's and accompanying tsunami's effects [Comte and Pardo, 1991]. Slip for both the Tocopilla and Antofagasta events taper beneath the peninsula. Assuming a fully locked interface here during the interseismic period, co-seismic slip tapering suggests a large slip deficit [Béjar-Pizarro *et al.*, 2010; Victor *et al.*, 2011], which has not been compensated for despite significant afterslip (Figure 8) in the months and years following the Antofagasta earthquake [Chlieh *et al.*, 2004; Pritchard and Simons, 2006]. At the latitude of MP, aftershocks protrude offshore, whereas onshore seismicity is sparse and the downdip limit of seismicity tends to terminate at a shallower depth (Figure 8 vertical N-S section). Together this gives the impression that the band of aftershocks skirt around MP. The distinct pattern of aftershock seismicity and aseismic slip makes the case that the interface exhibits stable

frictional or ductile behavior below and toward the east of MP causing the updip excursion of the lower termination of seismicity and aseismic slip pulses. In turn the vigorous aftershock seismicity along the coast of MP and further seaward, and the occurrence of some co-seismic slip and afterslip offshore MP might indicate conditionally stable behavior here following the reasoning given above for the deep Tocopilla aftershock area. Hence, the offshore protrusion of conditionally stable behavior at the latitude of MP might serve at least occasionally, under favorable conditions (i.e., high pore fluid pressures), as a barrier to earthquake ruptures north and south of MP. However, this together with the possibility that the Tocopilla rupture might well be stalled by the stress shadow left behind by the Antofagasta earthquake leaves the question open, whether MP is a persistent or occasional barrier at the million-year time scale.

[24] The plate interface beneath MP, however, is not completely aseismic. There is a lineament of events, where both aftershock sequences abut (see black arrow on the north-south depth cross section in Figure 8). It is very suggestive that this line marks the boundary between the two ruptures. We note here that this lineament is not the one described in Victor *et al.* [2011], which is located further south. If this boundary would represent a strike-slip fault, it could decouple the two plate segments. To check this possibility we calculated source mechanisms for events along the lineament. As data coverage and quality for these particular Tocopilla aftershocks did not allow retrieval of source parameters we resorted to the Antofagasta data set for which the dense station network allows for well determined first motion fault plane solutions (Figure 10). Practically all events we looked at show pure north-south striking thrust mechanisms, many of them with one shallow-dipping nodal plane indicating slip on the subduction interface, rather than strike-slip faulting. Hence the nature of this boundary remains elusive.

[25] The simplest explanation for the observation that the combined Antofagasta and Tocopilla aftershock series skirt around MP is that the downdip end of the seismogenic zone shallows beneath MP. As the dip of the slab changes only gradually and is even a few degrees smaller below Mejillones (Figure 9), the updip shift of the downdip limit of the seismogenic zone requires a significantly shallower continental Moho, if the downdip limit of the seismogenic zone is also controlled by the intersection with the continental Moho (Figure 9). To test this hypothesis we revisited Husen *et al.*'s [2000] tomography model and plotted a cross section along a north-south line approximately paralleling the base of the transition zone where the slab presumably intersects the continental Moho (Figure 11, see Figure 10 for location). If we take the 7.5 km/sec *P* velocity isoline as a proxy for the Moho this corresponds well with the deepest Antofagasta aftershocks and thickness of the crust beneath the Coastal Cordillera [Bock *et al.*, 2000; Patzwahl *et al.*, 1999]. The base of the crust as indicated by the 7.5 km/s contour shallows beneath MP by about 8 km. Assuming an 18° dip of the slab, an eight kilometer shallower Moho would shift the intersection of the slab horizontally in the updip direction by about 25 km. This is similar to the width of the peninsula and the amount of updip deviation of the band of seismicity (Figure 9). Resolution of the tomographic model is good for the discussed depth and longitude [Husen *et al.*, 2000], but

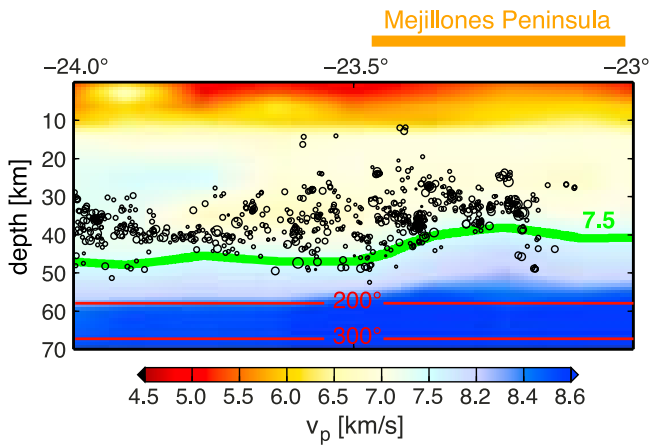


Figure 11. North-south cross section through the tomographic model of *Husen et al.* [2000] along approximately the downdip end of the seismogenic zone (see Figure 10 for location). The green line is the isoline for $v_p = 7.5$ km/s as a proxy for the Moho. The approximate extent of Mejillones Peninsula is indicated on top. Circles are aftershocks of the 1995 Antofagasta earthquake used in the local earthquake tomography. Lower plate isotherms at this latitude are from *Springer* [1999].

diminishes to the north, because the inversion used only aftershocks of the Antofagasta event. Additional seismic data, i.e., from the Tocopilla aftershock series, and possibly gravity data should be used to verify Moho depth across MP.

[26] The rather flat surface of MP and its moderately dipping ($\sim 5^\circ$) offshore submarine toe also form a first order bathymetric/topographic anomaly separating the two forearc segments to the north and south. Those segments, in contrast to the bathymetric/topographic profile at the latitude of MP, exhibit a downdip segmentation, i.e., a steep ($\sim 10^\circ$) dipping submarine outer slope, flat shelf basins offshore and a Coastal Cordillera onshore (Figure 9). The latter, as well as an associated coastal escarpment, are less developed in the hinterland of MP. While the areas near the trench are void of seismicity during the observation period, great megathrust earthquake slip (during the 1995 Antofagasta earthquake) as well as inter-seismic backslip (due to locking of the plate interface and to be released during future great earthquakes) tends to show a maximum underneath the shelf basins north and south of the MP (Figure 9). The distinct bathymetric/topographic profile as well as a generally higher rate of deformation of the wedge both in the long term [*Victor et al.*, 2011] and the short-term (Figure 7) at the latitude of MP point to differing strength of either the interface, its hanging wall or both compared to its neighboring segments.

6.4. Downdip Segmentation of the Seismogenic Zone

[27] Based on our observations, the seismogenic zone north and south of MP is segmented in the updip direction to first order into (1) an aseismic creeping zone at depth where the slab is capped by the hydrated mantle wedge, (2) a partially locked transitional zone beneath the Coastal Cordillera characterized by moderate to large earthquakes in a conditionally stable regime and possibly with spatially heterogeneous and incomplete stress drops as suggested by abundant aftershock seismicity and afterslip and (3) an offshore zone

dominated by unstable frictional behavior that is either locked or slips in great earthquakes where stress drop is presumably more homogenous and complete and aftershock activity therefore absent (seismic coupling coefficient $\chi = 1$, Figure 9). The latter might in most cases not reach the trench because of (4) a very shallow largely aseismic behavior [*Bilek and Lay*, 2002]. While ruptures of infrequent great ($M > 8$) earthquakes extend much farther offshore, most large ($M < 8$) events occur in the proposed transition zone, accompanied by abundant smaller earthquakes (mainly during aftershock series) and possibly aseismic slip during the inter-seismic period. Quite clearly, the upper limit of this proposed transition zone parallels the coastline in the region of the Tocopilla and Antofagasta earthquakes. This correlation as well as the first-order downdip segmentation described here appears to be a more general feature in the South American subduction zone, as is demonstrated in Figure 12, which shows well-determined slip distributions (all including geodetic data) of recent large earthquakes in Chile (this study) [*Chlieh et al.*, 2004; *Moreno et al.*, 2012] and Peru [*Pritchard et al.*, 2007; *Pritchard and Fielding*, 2008]. This is particularly obvious in places where the coastline is not parallel to the trench as in the case of the 2007 Pisco earthquake in Peru [*Sladen et al.*, 2010]. Large earthquakes ($7 < M < 8$, red slip contours in Figure 12) break the narrow transition zone. In this respect the 1997 Peru and 2007 Tocopilla earthquakes are comparable to each other. We also note here the recent finding that coherent co-seismic high frequency radiation for large earthquakes appears to be consistently displaced downdip of the high slip regions [*Koper et al.*, 2011, 2012]. For the M8.8 2010 Maule earthquake, e.g., high frequency wave radiation was imaged beneath the coastline whereas high slip occurred offshore [*Koper et al.*, 2012]. This observation might also be ascribed to the downdip changes in frictional properties suggested here.

[28] The spatial correlation of seismogenic zone segmentation and topography suggests a causal relationship. *Ruff and Tichelaar* [1996] first pointed out a general correlation of the downdip limit of the seismogenic zone and the coastline and attributed this to the intersection of the slab with the forearc, continental Moho which for normal crustal thickness, density and isostasy coincides with elevations just above sea level. Here, however, we argue that with the thick South American crust, the intersection of the slab with the continental Moho occurs well landward of the coastline, and it is the boundary between areas of frictionally unstable behavior, which are inter-seismically completely locked and break in great earthquakes in a stick-slip manner, and a transition zone characterized by conditionally stable behavior and partial locking that correlates with the coastline.

[29] Although co-seismic deformation induced by the 2007 Tocopilla earthquake uplifted the coastal area, this deformation is presumably elastic and will not be preserved over the next seismic cycle. Moreover, the 1995 Antofagasta earthquake did not uplift the coastal area, nor would any great earthquake rupturing the currently locked zone updip of the Tocopilla earthquake. Instead we suggest that upper plate compression related to the downdip gradient in locking in the transition zone is responsible for long-term permanent uplift of the coastline as has been observed in analogue models of elastoplastic seismic cycles [*Rosenau and*

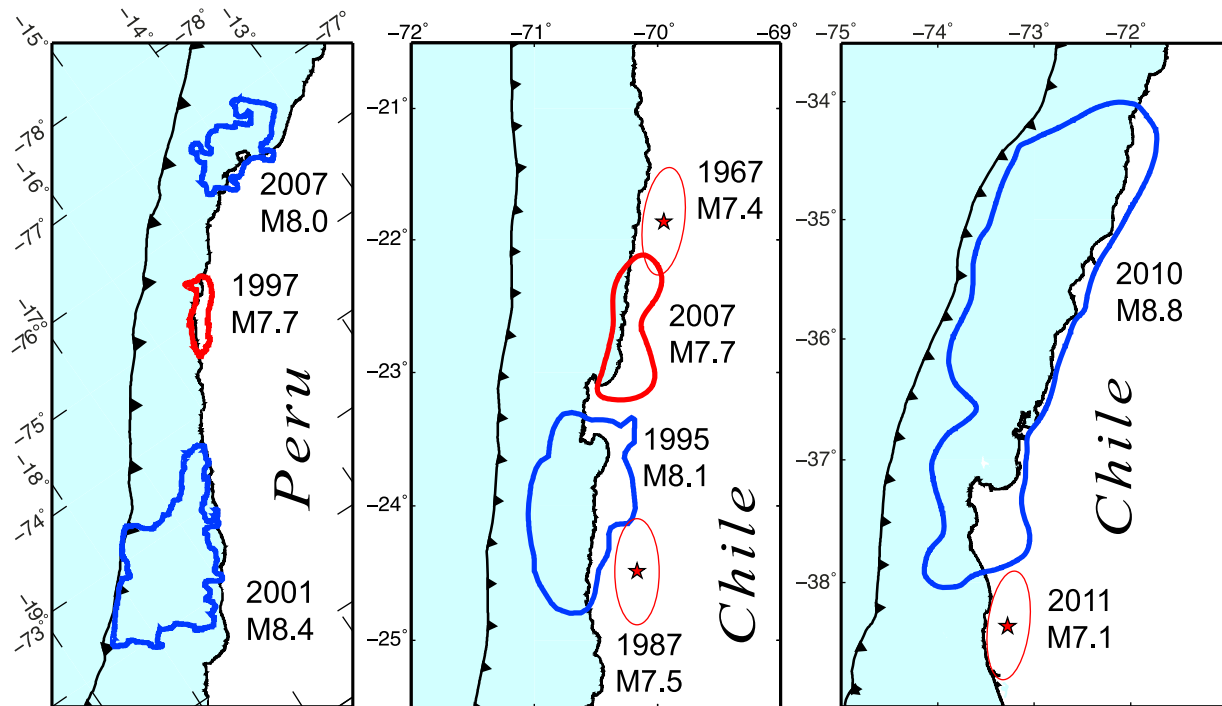


Figure 12. Trench, coastline and slip for events with $M > 8$ (blue) and $7 < M < 8$ (red) for southern Peru, northern Chile and south-central Chile. Slip models for Peru events are from *Pritchard et al.* [2007] and *Pritchard and Fielding* [2008], for the 1995 Antofagasta earthquake from *Chlieh et al.* [2004] and for the 2010 Maule earthquake from *Moreno et al.* [2012]. Slip distributions for the Maule event vary between different studies. We plot here the one that uses the most complete geodetic data set, because geodetic data are the most sensitive in defining the downdip limit of slip.

Oncken, 2009]. If the downdip limit of the locked zone is spatially stable over many seismic cycles (as it would be if it is controlled by temperature or Moho) a small fraction (few percent) of the inter-seismic shortening accumulated as permanent upper plate thickening would suffice to reconcile observed long-term coastal uplift rates (< 1 mm/a) and thus contribute to the emergence of land and the formation of a coastal cordillera over geologic timescales. In our study area at around 23°S , the long-term permanent coastal uplift rate, accumulated over many seismic cycles, is about 0.24 mm/a [*Ortlieb et al.*, 1996].

[30] In the elastoplastic subduction earthquake cycle models of *Rosenau and Oncken* [2009] shortening within the wedge localizes over multiple seismic cycles at the periphery of the stick-slip zone due to co-seismic compression at the updip limit and inter-seismic compression at the downdip limit. Over geological time scales (100 ka – Ma) zones of permanent uplift are therefore predicted to encompass stable forearc basins, which correlate spatially (and causally) with the frictionally unstable areas along the plate interface. This kind of “seismotectonic” forearc segmentation is clearly visible in the cross-sections of the submarine forearc wedges at 22.5°S and 24°S through the northern Tocopilla and the southern Antofagasta ruptures (Figure 9). Formation of a rather undeformed platform or basin above the frictionally unstable subduction interface has been theoretically explained with the dynamic Coulomb wedge theory [*Wang and Hu*, 2006] and forearc basins have been found globally to overlie regions of large slip due to subduction

earthquakes [*Song and Simons*, 2003; *Wells et al.*, 2003]. Spatial correlation between slip, aftershocks and forearc basin-outer slope transition has also been found at the updip limit of the ruptures of the great 2004 Aceh and 2005 Nias earthquakes [*Tilmann et al.*, 2010].

6.5. Morphotectonic Analysis

[31] In order to further investigate the nature of accumulation of long-term permanent deformation over various time scales, especially the emergence of the coastline and peninsula, and its possible relation to slip regimes along the plate interface we here apply the critical wedge theory [*Dahlen et al.*, 1984; *Davis et al.*, 1983]. We base our analysis on a generic model of seismotectonic deformation of a forearc wedge including the evaluation of wedge stability as a function of basal friction and pore fluid pressure. The latter have been varied to represent different stages of the megathrust seismic cycle. The following simplifying assumptions and premises, where possible constrained by observations, are needed: (1) The study area is segmented into either flat and internally undeformed “platforms,” i.e., the shelf basins north and south of MP. These platforms are associated on the trench side with seaward dipping outer slopes ($\beta \sim 10^{\circ}$) characterized by extension. Or it represents a “peninsula” which is flat onshore and dips continuously at 5° offshore where normal faulting also occurs. (2) The continental forearc wedge deforms in a brittle manner at all timescales and is mechanically homogenous and cohesionless (internal friction angle $\Phi_w = 30^{\circ}$, density $\rho = 2500$ kg/m³). (3) The megathrust

has uniform dip ($\alpha = 20^\circ$) and the basal static friction angle is 5° smaller than in the overlying wedge ($\Phi_b = 25^\circ$). (4) The plate interface obeys a rate-and-state frictional behavior including persistent areas of velocity weakening ($a-b < 0$, [e.g., Scholz, 1998]) and its counterpart rate strengthening ($a-b > 0$). A temporal transition between seismic and aseismic slip at a given place is then diagnostic of the so-called “conditionally” stable regime [e.g., Scholz, 1998]. This frictional regime is characterized by intrinsic velocity weakening ($a-b < 0$) but slip stability is controlled by deformation rate (low rates favoring stable slip) or normal load (low loads favoring stable slip). (5) Deformation is plane strain and represented by a 2D model. (6) Pore fluid pressure is either near hydrostatic (fluid-to-lithostatic pressure ratio $\lambda = 0.4$) or near lithostatic ($\lambda = 0.9$) and is the same within the wedge as at its base. The second part of the last assumption, i.e., that fluid pressure is the same in the shear zone and the hanging wall, is probably not always true, particularly at the downdip end of the seismogenic zone, where it is hypothesized that at least transient sealing between upper and lower plate occurs [Audet et al., 2009; Song et al., 2009], leading to asynchronous changes in fluid pressure, as will be discussed below. The morphotectonic analysis that follows consists of an evaluation of the position of the segments in the $\alpha - \beta$ space relative to stability fields calculated using the analytical solutions for the critical wedge problem [Dahlen et al., 1984; Lehner, 1986]. The size and shape of a stability field is determined by variations in Φ_b , simulating rate dependent changes in friction angle, and λ , simulating pore fluid pressure changes. Positions inside a stability field indicate a stable tectonic environment, positions above or below indicate unstable extensional and compressional regimes respectively. Pairs of α and β that fall on the border of a stability field are said to form the critical taper ($\alpha + \beta$) and represent a state in which the wedge is at the verge of failure.

[32] The seismotectonic behavior of the offshore regions north and south of the peninsula follow a common pattern, which can be explained by spatial-temporal changes in deformation rate and fluid pressure (Figures 13a and 13b). Accordingly, the observation of an absence of deformation of the platforms in combination with seismic stick-slip mode (100% seismic coupling, full locking, no creep) is consistent with an intrinsic velocity weakening property and low fluid pressures as the stability fields calculated for $\lambda = 0.4$ and for $\Phi_b < 25^\circ$ enclose their taper (red circle in Figure 13a). The combination of upper plate extension, evidenced by abundant normal faulting [von Huene and Ranero, 2003], and an absence of megathrust seismicity beneath the outer slopes suggests a velocity strengthening behavior in combination with variable pore fluid pressures here (Figure 13b). We view it as likely that high pore pressures triggering normal faulting here only occurs transiently during and/or after an earthquake due to static co-seismic elastic compression of the outer forearc and draining of deeper reservoirs [Wang et al., 2010].

[33] Megathrust slip at the latitude of the MP as well as below the coastline in general is accommodated by aftershock seismicity, triggered by slow slip and partial inter-seismic locking. The surface slopes realized along the coastline including MP are rather small ($<5^\circ$) and the areas

are characterized structurally by both shallow normal faulting (mainly offshore MP and the Coastal Escarpment) as well as coastal uplift. We attribute the latter to mild compression presumably realized transiently, but sufficient to lead to emergence over geological timescales [e.g., Victor et al., 2011]. In the framework of the model applied here, these observations and inferences require partitioning of deformation at sub-seismic cycle scale and are reconcilable only with conditionally stable behavior, i.e., velocity weakening and high pore fluid pressure, along the megathrust (Figures 13c and 13d). Accordingly, coastal areas, particularly those that are rather flat, are either critical or involve compressional deformation during the inter-seismic times, when megathrust slip is slow, resulting in relatively high basal strength (friction angles $>20^\circ$). In contrast, when slip rate increases (e.g., during episodic slip or moderate earthquakes) and basal strength drops (friction angles $<10^\circ$), coastal regions may enter the extensional regime, particularly those regions that have already acquired a significant slope ($\sim 5^\circ$). Depending on whether inter-seismic compressional uplift or episodic extensional subsidence dominates over many seismic cycles, net emergence or submergence of coastal areas over hundreds of thousands to millions of years will occur.

[34] We therefore suggest that coastal emergence and topography directly reflect the conditionally stable regime at depth. Transient near lithostatic pore fluid pressures in the transition zone controlling the conditionally stable conditions are described e.g., by Nippres and Rietbrock [2007]. In their analysis of the Antofagasta aftershock sequence they interpreted a near vertical streak penetrating the upper plate as being due to co-seismic hydro fracturing of the inter-seismically sealed subduction channel, allowing fluids to penetrate into the upper plate. This interpretation was assisted by the observation of a v_p/v_s anomaly that appeared approximately six weeks after the main shock in the upper plate in a time-sliced tomography [Husen and Kissling, 2001]. This v_p/v_s anomaly was also interpreted as migrating fluids pumped into the hanging wall following megathrust rupture [Husen and Kissling, 2001]. Slightly to the north, at $21^\circ S$, the ANCORP deep seismic profile revealed a dipping band of high reflectivity between 55 and 70 km depth that was interpreted as fluids trapped in the megathrust shear zone or just above [Oncken et al., 1999]. Geophysical signals that can be interpreted to reflect near-lithostatic fluid pressure in the subduction channel or oceanic crust along the downdip transition from locking to creeping have also been found in the Mexican [Song et al., 2009] and Cascadia [Audet et al., 2009] subduction zones from converted and reflected seismic waves. The downdip part of the seismogenic zone in both of these subduction zones, however, behaves in a fundamentally different manner to northern Chile by featuring episodic tremor and episodic slow slip behavior. In both of these subduction zones the relatively young and hot plates have temperatures above $350^\circ C$ in the transition zones [Wada and Wang, 2009], where plasticity of quartz and later feldspar commences and the deformation mechanism changes from frictional to viscous (rate strengthening). Hence, the peculiar behavior of the Chilean transition zone, with its large but not quite great earthquakes, inter- and post-seismic micro-seismicity, and afterslip may be attributed to a cold, velocity-weakening dominated

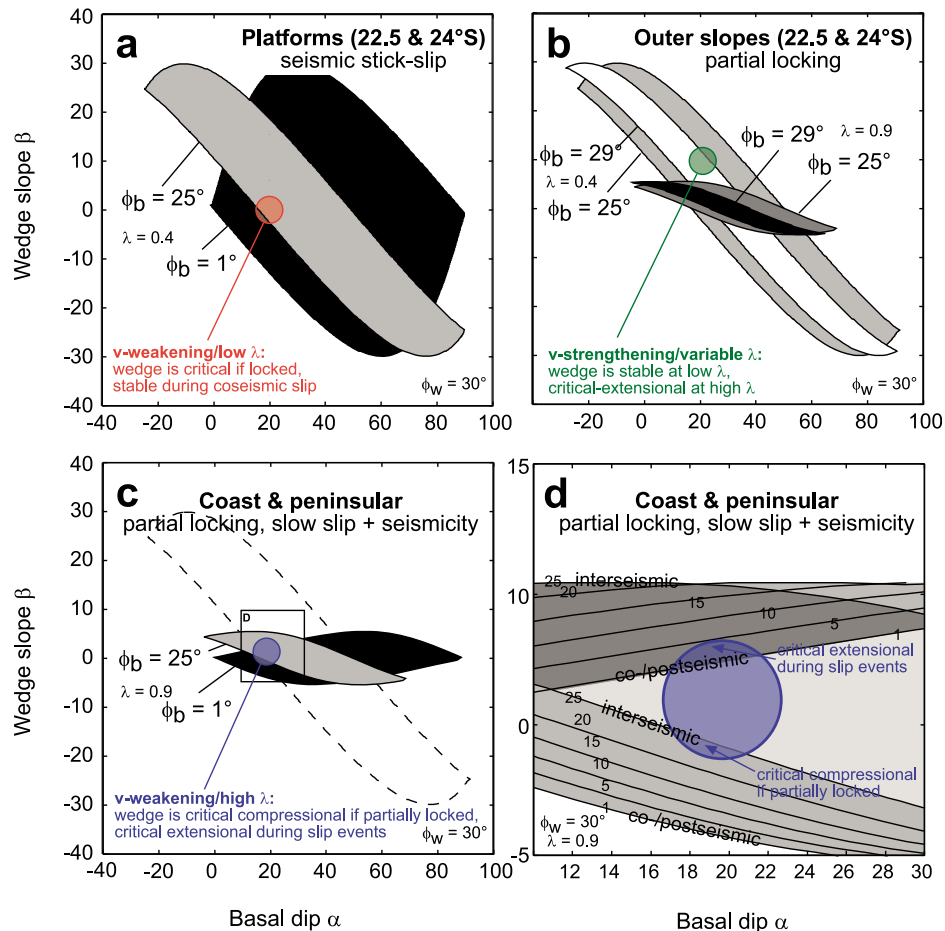


Figure 13. Morphotectonic analysis of seismotectonic observations using principles of the critical taper theory. Wedge stability fields in the $\alpha - \beta$ space calculated for (a) platforms, (b) outer slopes, (c) coastal regions (including Mejillones Peninsula), and (d) coastal regions with zoom. Colored circles represent geometries of the respective regions. In all plots wedge slope (β in degrees, seaward positive) is plotted on the y axis against basal megathrust dip (α in degrees, landward positive) on the x axis. $\alpha + \beta$ is the taper angle of the forearc wedge. Sigmoidal fields indicate “stable” geometries and enclose wedge tapers that would not deform internally under the given conditions. Taper angles falling above or below the stability fields belong to unstable geometries and indicate wedges undergoing compression and extension, respectively, in order to reach a stable geometry. Border line tapers mark “critical” geometries characterizing wedges that are exactly at the verge of failure but undeforming. Stability fields are calculated for variable basal friction angle ($1^\circ < \phi_b < 29^\circ$) and pore fluid pressure ratio (hydrostatic = $0.4 < \lambda < 0.9$ = near lithostatic) and constant wedge internal friction angle $\phi_w = 30^\circ$. Shaded stability fields are those discussed in the text, dashed stability field is for reference. Line numbers in Figure 13d represent different basal friction angles. According to our analysis (see text for details), under the given conditions, the forearc wedge underlying the tectonically stable (i.e., undeforming) platforms north and south of Mejillones Peninsula (Figure 13a) are inferred to overlie a megathrust characterized by velocity weakening and low (near hydrostatic) fluid pressure thus stabilizing the observed wedge geometry throughout most of the seismic cycle. In contrast the structure of outer slopes (Figure 13b) which are characterized by abundant normal faulting indicate that the wedge here reaches the extensional condition at least temporarily, most likely during periods of increased pore fluid pressure, for example during the post-seismic stage. Indications for both compression and extension during the seismic cycle in coastal areas (including Mejillones Peninsula) provide evidence for fluctuation between critical compressional and extensional conditions reconciled here in the proposed “conditionally stable” regime, i.e., velocity weakening at high near lithostatic fluid pressures. Extension then occurs during slow slip events and moderate ($M \leq 7$) earthquakes.

environment under high pore fluid pressures. In contrast, episodic tremor and episodic slow slip at the downdip limit of the seismogenic zone seems to be related to warm, brittle-ductile conditions, and also high pore fluid pressures.

[35] While the coastline itself, to first order, owes its existence to conditions favoring conditionally stable behavior below a certain depth (called transition here), peninsulas to a second order may be related to lateral changes of pore

pressure. Though the latter are controlled by structure in the first place (permeability, porosity) they might well be transient given their diffusive character. Consequently, peninsulas should not be regarded as all-time barriers to slip.

7. Conclusions

[36] We determined the slip distribution from near-field static surface deformation of the M_w 7.7 Tocopilla earthquake and relocated six months of pre-main shock and one week of aftershock activity. The Tocopilla earthquake and its aftershock sequence occurred in a transition zone between a totally locked portion of the megathrust and the intersection of the slab with the forearc Moho. Downdip of the intersection the plate interface creeps aseismically. Analyses of the 38 largest aftershocks using local and regional broadband waveforms show predominantly thrust mechanisms, consistent with motion along the plate interface. Some events offshore of Mejillones Peninsula, however, seem to have occurred in the upper plate and indicate normal faulting. Aftershocks of the neighboring 1995 Antofagasta earthquake also cluster in the transition zone, although the main shock ruptured mainly updip, in a segment that is totally locked during the inter-seismic period. The boundary between the locked zone and the transition zone parallels the coastline. This downdip segmentation of the megathrust appears to be a general feature along the South American plate boundary, where great earthquakes ($M > 8$) break the offshore part of the thrust with their downdip limits coinciding with the coastline, and large but not quite great earthquakes ($M < 8$) rupture in the transition zone. The coincidence of the downdip limit of large earthquakes with the coastline can be explained in that this is also the downdip boundary of the totally locked zone. Shortening then localizes in the overlying wedge during the inter-seismic period and therefore, in the long run, builds the topography that forms the coast.

[37] MP served as a barrier for both the 1995 Antofagasta and 2007 Tocopilla earthquakes. Their aftershock sequences suggest an E-W trending boundary beneath the peninsula that limits the aftershocks of each event to one side irrespective of Coulomb stress predictions. However, aftershocks delineating this boundary indicate slip on the megathrust, not on a strike-slip fault. The combined 1995 Antofagasta and 2007 Tocopilla aftershocks appear to skirt around MP in map view. This observation is most easily explained by downdip termination of seismicity at a shallower depth beneath MP that could be caused by, e.g., a shallower continental forearc Moho beneath MP and hence a shallower contact between the subducted slab and the mantle wedge. Support for this interpretation comes from a tomographic model of *Husen and Kissling* [2001]. The distinct pattern of aftershock seismicity, co- and post-seismic slip, and inter-seismic locking reveals both downdip and along strike segmentation of stable, unstable and conditionally stable frictional behavior. The variation of frictional behavior is reflected by the forearc wedge structure and geometry with coastal emergence related to conditionally stable slip behavior. The seismogenic behavior of the Chilean transition zone, featuring large but not quite great earthquakes, inter- and post-seismic micro-seismicity, and episodic after-

slip may be attributed to a cold, velocity weakening dominated environment under high pore fluid pressure.

[38] **Acknowledgments.** We thank the IPOC initiative for maintaining the seismic network and providing the high quality data used in this study. We thank J.-P. Avouac and N. Cubas for discussion and help with critical taper analysis. We are also grateful to G. Chong and G. Gonzalez for their support in the field. F. Sodoudi kindly provided receiver functions. We thank Jim Mechie for reading the manuscript and for helpful comments. We also thank two anonymous referees and the Associate Editor for their constructive reviews.

References

- Angermann, D., J. Klotz, and C. Reigber (1999), Space-geodetic estimation of the Nazca-South America Euler vector, *Earth Planet. Sci. Lett.*, *171*, 329–334, doi:10.1016/S0012-821X(99)00173-9.
- Armijo, R., and R. Thiele (1990), Active faulting in northern Chile: Ramp stacking and lateral decoupling along a subduction plate boundary?, *Earth Planet. Sci. Lett.*, *98*(1), 40–61, doi:10.1016/0012-821X(90)90087-E.
- Audet, P., M. G. Bostock, N. I. Christensen, and S. M. Peacock (2009), Seismic evidence for overpressured subducted oceanic crust and megathrust fault sealing, *Nature*, *457*(7225), 76–78, doi:10.1038/nature07650.
- Béjar-Pizarro, M., et al. (2010), Asperities and barriers on the seismogenic zone in north Chile: State-of-the-art after the 2007 Mw 7.7 Tocopilla earthquake inferred by GPS and InSAR data, *Geophys. J. Int.*, *183*(1), 390–406, doi:10.1111/j.1365-246X.2010.04748.x.
- Bilek, S. L., and T. Lay (2002), Tsunami earthquakes possibly widespread manifestations of frictional conditional stability, *Geophys. Res. Lett.*, *29*(14), 1673, doi:10.1029/2002GL015215.
- Bock, G., B. Schurr, and G. Asch (2000), High-resolution image of the oceanic mocho in the subducting Nazca Plate from P-S converted waves, *Geophys. Res. Lett.*, *27*(23), 3929–3932, doi:10.1029/2000GL011881.
- Bouchon, M. (1981), A simple method to calculate Green's functions for elastic layered media, *Bull. Seismol. Soc. Am.*, *71*(4), 959–971.
- Buske, S., S. Lüth, H. Meyer, R. Patzig, C. Reichert, S. Shapiro, P. Wigger, and M. Yoon (2002), Broad depth range seismic imaging of the subducted Nazca Slab, north Chile, *Tectonophysics*, *350*(4), 273–282, doi:10.1016/S0040-1951(02)00117-8.
- Chlieh, M., J.-B. de Chabaliér, J. C. Ruegg, R. Armijo, R. Dmowska, J. Campos, and K. L. Feigl (2004), Crustal deformation and fault slip during the seismic cycle in the north Chile subduction zone, from GPS and InSAR observations, *Geophys. J. Int.*, *158*(2), 695–711, doi:10.1111/j.1365-246X.2004.02326.x.
- Comte, D., and M. Pardo (1991), Reappraisal of great historical earthquakes in the northern Chile and southern Peru seismic gaps, *Nat. Hazards*, *4*(1), 23–44, doi:10.1007/BF00126557.
- Dahlen, F. A., J. Suppe, and D. Davis (1984), Mechanics of fold-and-thrust belts and accretionary wedges: Cohesive Coulomb theory, *J. Geophys. Res.*, *89*(B12), 10,087–10,101, doi:10.1029/JB089iB12p10087.
- Davis, D., J. Suppe, and F. A. Dahlen (1983), Mechanics of fold-and-thrust belts and accretionary wedges, *J. Geophys. Res.*, *88*, 1153–1172, doi:10.1029/JB088iB02p01153.
- Delouis, B., A. Cisternas, L. Dorbath, L. Rivera, and E. Kausel (1996), The Andean subduction zone between 22° and 25°S (northern Chile): Precise geometry and state of stress, *Tectonophysics*, *259*(1–3), 81–100, doi:10.1016/0040-1951(95)00065-8.
- Delouis, B., T. Monfret, L. Dorbath, M. Pardo, L. Rivera, D. Comte, H. Haessler, J. Caminade, L. Ponce, and E. Kausel (1997), The Mw = 8.0 Antofagasta (northern Chile) earthquake of 30 July 1995: A precursor to the end of the large 1877 gap, *Bull. Seismol. Soc. Am.*, *87*(2), 427.
- Delouis, B., M. Pardo, D. Legrand, and T. Monfret (2009), The Mw 7.7 Tocopilla earthquake of 14 November 2007 at the southern edge of the northern Chile seismic gap: Rupture in the deep part of the coupled plate interface, *Bull. Seismol. Soc. Am.*, *99*(1), 87–94, doi:10.1785/0120080192.
- Engdahl, E. R., R. D. van der Hilst, and R. Buland (1998), Global teleseismic earthquake relocation with improved travel times and procedures for depth determination, *Bull. Seismol. Soc. Am.*, *88*(3), 722–743.
- Giese, P., E. Scheuber, F. Schilling, M. Schmitz, and P. Wigger (1999), Crustal thickening processes in the central Andes and the different natures of the Moho-discontinuity, *J. South Am. Earth Sci.*, *12*(2), 201–220, doi:10.1016/S0895-9811(99)00014-0.
- Graeber, F. M., and G. Asch (1999), Three-dimensional models of P wave velocity and P-to-S velocity ratio in the southern central Andes by simultaneous inversion of local earthquake data, *J. Geophys. Res.*, *104*(B9), 20,237–20,256, doi:10.1029/1999JB900037.

- Helmstetter, A., and B. E. Shaw (2006), Relation between stress heterogeneity and aftershock rate in the rate-and-state model, *J. Geophys. Res.*, *111*, B07304, doi:10.1029/2005JB004077.
- Helmstetter, A., and B. E. Shaw (2009), Afterslip and aftershocks in the rate-and-state friction law, *J. Geophys. Res.*, *114*, B01308, doi:10.1029/2007JB005077.
- Husen, S., and E. Kissling (2001), Postseismic fluid flow after the large subduction earthquake of Antofagasta, Chile, *Geology*, *29*(9), 847–850, doi:10.1130/0091-7613(2001)029<0847:PFATL>2.0.CO;2.
- Husen, S., E. Kissling, E. Flueh, and G. Asch (1999), Accurate hypocentre determination in the seismogenic zone of the subducting Nazca Plate in northern Chile using a combined on-/offshore network, *Geophys. J. Int.*, *138*(3), 687–701, doi:10.1046/j.1365-246x.1999.00893.x.
- Husen, S., E. Kissling, and E. Flueh (2000), Local earthquake tomography of shallow subduction in north Chile: A combined onshore and offshore study, *J. Geophys. Res.*, *105*(B12), 28,183–28,198, doi:10.1029/2000JB900229.
- Hyndman, R., M. Yamano, and D. Oleskevich (1997), The seismogenic zone of subduction thrust faults, *Isl. Arc*, *6*(3), 244–260, doi:10.1111/j.1440-1738.1997.tb00175.x.
- Kaneko, Y., J. P. Avouac, and N. Lapusta (2010), Towards inferring earthquake patterns from geodetic observations of interseismic coupling, *Nat. Geosci.*, *3*(5), 363–369, doi:10.1038/ngeo843.
- Kelleher, J. A. (1972), Rupture zones of large South American earthquakes and some predictions, *J. Geophys. Res.*, *77*(11), 2087–2103, doi:10.1029/JB077i011p02087.
- Khazaradze, G., and J. Klotz (2003), Short- and long-term effects of GPS measured crustal deformation rates along the south central Andes, *J. Geophys. Res.*, *108*(B6), 2289, doi:10.1029/2002JB001879.
- Kissling, E., W. L. Ellsworth, D. Eberhart-Phillips, and U. Kradolfer (1994), Initial reference models in local earthquake tomography, *J. Geophys. Res.*, *99*(B10), 19,635–19,646, doi:10.1029/93JB03138.
- Koper, K. D., A. R. Hutko, T. Lay, C. J. Ammon, and H. Kanamori (2011), Frequency-dependent rupture process of the 2011 M w 9.0 Tohoku Earthquake: Comparison of short-period P wave backprojection images and broadband seismic rupture models, *Earth Planets Space*, *63*(7), 599–602, doi:10.5047/eps.2011.05.026.
- Koper, K. D., A. R. Hutko, T. Lay, and O. Sufri (2012), Imaging short-period seismic radiation from the 27 February 2010 Chile (M w 8.8) earthquake by back-projection of P, PP, and PKIKP waves, *J. Geophys. Res.*, *117*, B02308, doi:10.1029/2011JB008576.
- Lamb, S. (2006), Shear stresses on megathrusts: Implications for mountain building behind subduction zones, *J. Geophys. Res.*, *111*, B07401, doi:10.1029/2005JB003916.
- Lee, W. H. K., and C. J. Lahr (1975), HYPO71: A computer program for determining hypocenter, magnitude, and first motion pattern of local earthquakes, *U.S. Geol. Surv. Open File Rep.*, 75–331.
- Lehner, F. K. (1986), Comments on “Noncohesive critical Coulomb wedges: An exact solution,” *J. Geophys. Res.*, *91*, 793–796, doi:10.1029/JB091iB01p00793.
- Lin, J., and R. S. Stein (2004), Stress triggering in thrust and subduction earthquakes and stress interaction between the southern San Andreas and nearby thrust and strike-slip faults, *J. Geophys. Res.*, *109*, B02303, doi:10.1029/2003JB002607.
- Lorito, S., F. Romano, S. Atzori, X. Tong, A. Avallone, J. McCloskey, M. Cocco, E. Boschi, and A. Piatanesi (2011), Limited overlap between the seismic gap and coseismic slip of the great 2010 Chile earthquake, *Nat. Geosci.*, *3*(1), 1–5, doi:10.1038/ngeo1073.
- Loveless, J. P., M. E. Pritchard, and N. Kukowski (2010), Testing mechanisms of subduction zone segmentation and seismogenesis with slip distributions from recent Andean earthquakes, *Tectonophysics*, *495*(1–2), 15–33, doi:10.1016/j.tecto.2009.05.008.
- Madariaga, R., M. Métois, C. Vigny, and J. Campos (2010), Central Chile finally breaks, *Science*, *328*(5975), 181–182, doi:10.1126/science.1189197.
- Malgrange, M., and R. Madariaga (1983), Complex distribution of large thrust and normal fault earthquakes in the Chilean subduction zone, *Geophys. J. R. Astron. Soc.*, *73*(2), 489–505, doi:10.1111/j.1365-246X.1983.tb03326.x.
- McNally, K. (1983), Seismic gaps in space and time, *Annu. Rev. Earth Planet. Sci.*, *11*, 359–369, doi:10.1146/annurev.ea.11.050183.002043.
- Moreno, M., et al. (2012), Toward understanding tectonic control on the Mw 8.8 2010 Maule Chile earthquake, *Earth Planet. Sci. Lett.*, *321*–322, 152–165, doi:10.1016/j.epsl.2012.01.006.
- Motagh, M., B. Schurr, J. Anderssohn, B. Cailleau, T. R. Walter, R. Wang, and J.-P. Vilotte (2010), Subduction earthquake deformation associated with 14 November 2007, Mw 7.8 Tocopilla earthquake in Chile: Results from InSAR and aftershocks, *Tectonophysics*, *490*(1–2), 60–68, doi:10.1016/j.tecto.2010.04.033.
- Nábělek, J., and G. Xia (1995), Moment-tensor analysis using regional data: Application to the 25 March, 1993, Scotts Mills, Oregon, earthquake, *Geophys. Res. Lett.*, *22*(1), 13–16, doi:10.1029/94GL02760.
- Newman, A. V., G. Hayes, Y. Wei, and J. Convers (2011), The 25 October 2010 Mentawai tsunami earthquake, from real-time discriminants, finite-fault rupture, and tsunami excitation, *Geophys. Res. Lett.*, *38*, L05302, doi:10.1029/2010GL046498.
- Nippres, S. E. J., and A. Rietbrock (2007), Seismogenic zone high permeability in the central Andes inferred from relocations of micro-earthquakes, *Earth Planet. Sci. Lett.*, *263*(3–4), 235–245, doi:10.1016/j.epsl.2007.08.032.
- Nishenko, S. (1985), Seismic potential for large and great interplate earthquakes along the Chilean and Peruvian margins of South America: A quantitative reappraisal, *J. Geophys. Res.*, *90*, 3589–3615, doi:10.1029/JB090iB05p03589.
- Oleskevich, D., R. Hyndman, and K. Wang (1999), The updip and downdip limits to great subduction earthquakes: Thermal and structural models of Cascadia, south Alaska, SW Japan, and Chile, *J. Geophys. Res.*, *104*(B7), 14,965–14,991, doi:10.1029/1999JB900060.
- Oncken, O., et al. (1999), Seismic reflection image revealing offset of Andean subduction-zone earthquake locations into oceanic mantle, *Nature*, *397*(6717), 341–344, doi:10.1038/16909.
- Ortlieb, L., C. Zazo, J. L. Goy, C. Hillaire-Marcel, B. Ghaleb, and L. Cournoyer (1996), Coastal deformation and sea-level changes in the northern Chile subduction area (23 S) during the last 330 kyr, *Quat. Sci. Rev.*, *15*(8–9), 819–831, doi:10.1016/S0277-3791(96)00066-2.
- Patzwahl, R., J. Mechie, A. Schulze, and P. Giese (1999), Two-dimensional velocity models of the Nazca plate subduction zone between 19.5°S and 25°S from wide-angle seismic measurements during the CINCAS95 project, *J. Geophys. Res.*, *104*(B4), 7293–7317, doi:10.1029/1999JB900008.
- Peyrat, S., R. Madariaga, E. Buforn, J. Campos, G. Asch, and J.-P. Vilotte (2010), Kinematic rupture process of the 2007 Tocopilla earthquake and its main aftershocks from teleseismic and strong-motion data, *Geophys. J. Int.*, *182*, 1411–1430, doi:10.1111/j.1365-246X.2010.04685.x.
- Pritchard, M. E., and E. J. Fielding (2008), A study of the 2006 and 2007 earthquake sequence of Pisco, Peru, with InSAR and teleseismic data, *Geophys. Res. Lett.*, *35*, L09308, doi:10.1029/2008GL033374.
- Pritchard, M. E., and M. Simons (2006), An aseismic slip pulse in northern Chile and along-strike variations in seismogenic behavior, *J. Geophys. Res.*, *111*, B08405, doi:10.1029/2006JB004258.
- Pritchard, M. E., C. Ji, and M. Simons (2006), Distribution of slip from 11 M w > 6 earthquakes in the northern Chile subduction zone, *J. Geophys. Res.*, *111*, B10302, doi:10.1029/2005JB004013.
- Pritchard, M. E., E. O. Norabuena, C. Ji, R. Boroschek, D. Comte, M. Simons, T. H. Dixon, and P. A. Rosen (2007), Geodetic, teleseismic, and strong motion constraints on slip from recent southern Peru subduction zone earthquakes, *J. Geophys. Res.*, *112*, B03307, doi:10.1029/2006JB004294.
- Rosenau, M., and O. Oncken (2009), Fore-arc deformation controls frequency-size distribution of megathrust earthquakes in subduction zones, *J. Geophys. Res.*, *114*, B10311, doi:10.1029/2009JB006359.
- Ruff, L., and B. W. Tichelaar (1996), What controls the seismogenic plate interface in subduction zones?, in *Subduction Top to Bottom*, *Geophys. Monogr. Ser.*, vol. 96, edited by G. Bebout et al., pp. 105–111, AGU, Washington, D. C., doi:10.1029/GM096p0105.
- Scholz, C. H. (1998), Earthquakes and friction laws, *Nature*, *391*(6662), 37–42, doi:10.1038/34097.
- Schurr, B., and A. Rietbrock (2004), Deep seismic structure of the Atacama basin, northern Chile, *Geophys. Res. Lett.*, *31*, L12601, doi:10.1029/2004GL019796.
- Schwartz, S. Y., and J. M. Rokosky (2007), Slow slip events and seismic tremor at circum-Pacific subduction zones, *Rev. Geophys.*, *45*, RG3004, doi:10.1029/2006RG000208.
- Simons, M., S. E. Minson, A. Sladen, F. Ortega, J. Jiang, S. E. Owen, L. Meng, J. P. Ampuero, S. Wei, and R. Chu (2011), The 2011 magnitude 9.0 Tohoku-Oki earthquake: Mosaicking the megathrust from seconds to centuries, *Science*, *332*(6036), 142–1425, doi:10.1126/science.1206731.
- Sladen, A., H. Tavera, M. Simons, J. P. Avouac, A. O. Konca, H. Perfettini, L. Audin, E. J. Fielding, F. Ortega, and R. Cavagnoud (2010), Source model of the 2007 M w 8.0 Pisco, Peru earthquake: Implications for seismogenic behavior of subduction megathrusts, *J. Geophys. Res.*, *115*, B02405, doi:10.1029/2009JB006429.
- Sodoudi, F., X. Yuan, G. Asch, and R. Kind (2011), High-resolution image of the geometry and thickness of the subducting Nazca lithosphere beneath northern Chile, *J. Geophys. Res.*, *116*, B04302, doi:10.1029/2010JB007829.
- Song, T.-R. A., and M. Simons (2003), Large trench-parallel gravity variations predict seismogenic behavior in subduction zones, *Science*, *301*(5633), 630–633, doi:10.1126/science.1085557.

- Song, T.-R. A., D. V. Helmberger, M. R. Brudzinski, R. W. Clayton, P. Davis, X. Pérez-Campos, and S. K. Singh (2009), Subducting slab ultra-slow velocity layer coincident with silent earthquakes in southern Mexico, *Science*, *324*(5926), 502–506, doi:10.1126/science.1167595.
- Springer, M. (1999), Interpretation of heat-flow density in the central Andes, *Tectonophysics*, *306*(3–4), 377–395, doi:10.1016/S0040-1951(99)00067-0.
- Tilman, F. J., T. J. Craig, I. Grevemeyer, B. Suwargadi, H. Kopp, and E. Flueh (2010), The updip seismic/aseismic transition of the Sumatra megathrust illuminated by aftershocks of the 2004 Aceh-Andaman and 2005 Nias events, *Geophys. J. Int.*, *181*, 1261–1274, doi:10.1111/j.1365-246X.2010.04597.x.
- Toda, S., R. S. Stein, K. Richards-Dinger, and S. Bozkurt (2005), Forecasting the evolution of seismicity in southern California: Animations built on earthquake stress transfer, *J. Geophys. Res.*, *110*, B05S16, doi:10.1029/2004JB003415.
- Victor, P., M. Sobiesiak, J. Glodny, S. N. Nielsen, and O. Oncken (2011), Long-term persistence of subduction earthquake segment boundaries: Evidence from Mejillones Peninsula, northern Chile, *J. Geophys. Res.*, *116*, B02402, doi:10.1029/2010JB007771.
- von Huene, R., and C. Ranero (2003), Subduction erosion and basal friction along the sediment-starved convergent margin off Antofagasta, Chile, *J. Geophys. Res.*, *108*(B2), 2079, doi:10.1029/2001JB001569.
- Wada, I., and K. Wang (2009), Common depth of slab-mantle decoupling: Reconciling diversity and uniformity of subduction zones, *Geochem. Geophys. Geosyst.*, *10*, Q10009, doi:10.1029/2009GC002570.
- Waldhauser, F., and W. L. Ellsworth (2000), A double-difference earthquake location algorithm: Method and application to the northern Hayward fault, California, *Bull. Seismol. Soc. Am.*, *90*(6), 1353–1368, doi:10.1785/0120000006.
- Wang, K., and Y. Hu (2006), Accretionary prisms in subduction earthquake cycles: The theory of dynamic Coulomb wedge, *J. Geophys. Res.*, *111*, B06410, doi:10.1029/2005JB004094.
- Wang, R., F. Lorenzo Martin, and F. Roth (2003), Computation of deformation induced by earthquakes in a multi-layered elastic crust—FORTRAN programs EDGRN/EDCMP, *Comput. Geosci.*, *29*(2), 195–207, doi:10.1016/S0098-3004(02)00111-5.
- Wang, K., Y. Hu, R. von Huene, and N. Kukowski (2010), Interplate earthquakes as a driver of shallow subduction erosion, *Geology*, *38*(5), 431–434, doi:10.1130/G30597.1.
- Wang, R., B. Schurr, C. Milkereit, Z. Shao, and M. Jin (2011), An improved automatic scheme for empirical baseline correction of digital strong-motion records, *Bull. Seismol. Soc. Am.*, *101*(5), 2029–2044, doi:10.1785/0120110039.
- Wells, R. E., R. J. Blakely, Y. Sugiyama, D. W. Scholl, and P. A. Dinterman (2003), Basin-centered asperities in great subduction zone earthquakes: A link between slip, subsidence, and subduction erosion, *J. Geophys. Res.*, *108*(B10), 2507, doi:10.1029/2002JB002072.
- Wigger, P., et al. (1994), Variation in the crustal structure of the southern central Andes deduced from seismic refraction investigations, in *Tectonics of the Southern Central Andes*, edited by K. J. Reutter, E. Scheuber, and P. Wigger, pp. 23–48, Springer, New York, doi:10.1007/978-3-642-77353-2_2.